© 2015. Published by The Company of Biologists Ltd | Development (2015) 142, 2981-2995 doi:10.1242/dev.120469

RESEARCH ARTICLE

Epithelial inactivation of *Yy1* abrogates lung branching morphogenesis

Olivier Boucherat[1,*], Kim Landry-Truchon[1], Félix-Antoine Bérubé-Simard[1], Nicolas Houde[1], Laurent Beuret[1], Guillaume Lezmi[2,3], William D. Foulkes[4], Christophe Delacourt[2,3], Jean Charron[1] and Lucie Jeannotte[1,‡]

ABSTRACT

Yin Yang 1 (YY1) is a multifunctional zinc-finger-containing transcription factor that plays crucial roles in numerous biological processes by selectively activating or repressing transcription, depending upon promoter contextual differences and specific protein interactions. In mice, *Yy1* null mutants die early in gestation whereas *Yy1* hypomorphs die at birth from lung defects. We studied how the epithelial-specific inactivation of *Yy1* impacts on lung development. The *Yy1* mutation in lung epithelium resulted in neonatal death due to respiratory failure. It impaired tracheal cartilage formation, altered cell differentiation, abrogated lung branching and caused airway dilation similar to that seen in human congenital cystic lung diseases. The cystic lung phenotype in *Yy1* mutants can be partly explained by the reduced expression of *Shh*, a transcriptional target of YY1, in lung endoderm, and the subsequent derepression of mesenchymal *Fgf10* expression. Accordingly, SHH supplementation partially rescued the lung phenotype *in vitro*. Analysis of human lung tissues revealed decreased YY1 expression in children with pleuropulmonary blastoma (PPB), a rare pediatric lung tumor arising during fetal development and associated with *DICER1* mutations. No evidence for a potential genetic interplay between murine *Dicer* and *Yy1* genes during lung morphogenesis was observed. However, the cystic lung phenotype resulting from the epithelial inactivation of *Dicer* function mimics the *Yy1* lung malformations with similar changes in *Shh* and *Fgf10* expression. Together, our data demonstrate the crucial requirement for YY1 in lung morphogenesis and identify *Yy1* mutant mice as a potential model for studying the genetic basis of PPB.

KEY WORDS: YY1, SHH, FGF10, DICER1, Lung branching, Pleuropulmonary blastoma

INTRODUCTION

YY1 is a ubiquitous zinc finger transcription factor that contains diverse domains, enabling a plethora of protein-protein interactions. YY1 can recruit co-activators or co-repressors, which determine whether YY1 will execute inhibitory or activating functions on targets (Deng et al., 2010). In regulating a multitude of genes, YY1 plays crucial functions in numerous biological processes, including cell proliferation and differentiation, X-chromosome inactivation, and embryogenesis (Donohoe et al., 2007; Nicholson et al., 2011). The *Yy1* null mutation in mice results in peri-implantation lethality, a phenotype precluding investigation of YY1 requirement at later developmental stages (Donohoe et al., 1999). Using mouse lines carrying a *Yy1* conditional allele and tissue-specific *Cre*-expressing transgenes, *Yy1* was found to widely participate in developmental processes. However, despite the fact that mice expressing 25% of normal YY1 levels die at birth from respiratory failure due to collapsed lungs, little is known about the role of *Yy1* in lung morphogenesis (Affar et al., 2006).

Lung development is subdivided into five overlapping periods (Morrisey and Hogan, 2010). The embryonic phase is characterized by the formation of the ventral diverticulum that arises from the laryngotracheal groove of the foregut endoderm. Subsequently, this diverticulum, destined to become the trachea, divides into the left and right lung buds. At the pseudoglandular stage, the two primary buds elongate and undergo stereotypical branching via complex epithelium-mesenchyme interactions to form the respiratory tree. This is followed by the canalicular and saccular stages, during which the progressive differentiation of the pulmonary epithelium, the expansion of the vasculature with thinning of the mesenchyme, and the formation of functional air-blood barriers happen. Alveologenesis occurs after birth and is characterized by the formation of alveoli, the final gas-exchange units. Recent data indicate that the transition from branching morphogenesis to epithelial cell differentiation depends on control mechanisms involving key players of lung development such as Fgf10 and SOX9. These latter act by regulating the delicate balance between distal and proximal endodermal progenitors, promoting branching and preventing precocious alveolar differentiation (Chang et al., 2013; Volckaert et al., 2013; Yang and Chen, 2014).

We showed that the specific ablation of *Yy1* function in lung mesenchyme causes neonatal death of mutant pups due to collapsed lungs, a phenotype similar to that of *Yy1* hypomorph mutants (Bérubé-Simard et al., 2014). In the present study, we investigated the impact of the epithelial-specific inactivation of *Yy1* in the developing lung. The loss of *Yy1* function in lung epithelium also resulted in death at birth. It affected tracheal cartilage formation, cell differentiation and lung branching, leading to the formation of large cysts. The reduced expression of *Shh* and the subsequent upregulation of *Fgf10* expression likely contributed to the branching defects in *Yy1* mutants. Accordingly, *in vitro* SHH supplementation partially rescued the lung phenotype of *Yy1* mutant explants. The cysts in *Yy1* mutants mimicked the lung phenotype of *Dicer* mutants with similar *Shh* and *Fgf10* expression variations (Harris et al., 2006). DICER is a ribonuclease III essential for the biogenesis of mature microRNAs (Bartel, 2004). Cystic lesions characterize several pulmonary diseases such as congenital cystic adenomatoid malformation (CCAM) and pleuropulmonary blastoma (PPB), the latter being a rare dysontogenetic neoplasm

[1]Centre de Recherche sur le Cancer de l'Université Laval; CRCHUQ, L'Hôtel-Dieu de Québec, Québec, G1R 3S3, Canada. [2]AP-HP, Hôpital Necker-Enfants Malades, Service de Pneumologie Pédiatrique, Université Paris-Descartes, Paris, 75015, France. [3]Inserm U955, IMRB, Equipe 04, Créteil, 94011, France. [4]Department of Medical Genetics, Lady Davis Institute and Segal Cancer Centre, Jewish General Hospital, Montréal, H3G 1A4, Canada.
*Present address: CRIUCPQ, Québec, G1V 4G5, Canada.

‡Author for correspondence (lucie.jeannotte@crhdq.ulaval.ca)

Received 1 December 2014; Accepted 18 June 2015

Development (2015) 142, 2981-2995 doi:10.1242/dev.120469

of childhood evolving from a cystic to a solid state over time. Mutations in the human *DICER1* gene are found in PPB patients (Hill et al., 2008; Messinger et al., 2015). Analysis of lung tissue from CCAM patients revealed no major changes in YY1 expression. Conversely, decreased YY1 expression was detected in PPB children. In summary, our results demonstrate the essential requirement for YY1 in lung morphogenesis and identify YY1 as a potential factor involved in the molecular pathogenesis of PPB.

RESULTS

Loss of epithelial *Yy1* function causes defective lung morphogenesis

To circumvent the early embryonic lethality of the *Yy1* null mutants and address *Yy1* function in lung morphogenesis, we specifically deleted the *Yy1* gene in lung epithelium using the $Shh^{+/Cre}$ deleter mouse line (supplementary material Fig. S1; Harfe et al., 2004). All $Yy1^{flox/flox}$;$Shh^{+/Cre}$ newborns died at birth from respiratory failure, whereas $Yy1^{+/flox}$;$Shh^{+/Cre}$ mice were viable and normal (Table 1). Analysis of lungs from embryonic (E) day 18.5 $Yy1^{flox/flox}$;$Shh^{+/Cre}$ embryos revealed a disorganized architecture with the presence of dilated fluid-filled sacs (Fig. 1). At E12.5, lungs from $Yy1^{flox/flox}$;$Shh^{+/Cre}$ embryos presented two hypoplastic lobes in contrast to the expected asymmetric pattern of four right lobes and one left lobe. Moreover, lung epithelium of mutant specimens had an abnormal stratified structure.

To identify the causes of the lung phenotype, we looked at cell proliferation. At E12.5, reduced immunostaining for cyclin D1, a marker for the G1/S transition, for BrdU, which labels cells in S-phase, and for pHH3, a marker for cells in late G2 and mitosis, was specifically observed in lung epithelium of $Yy1^{flox/flox}$;$Shh^{+/Cre}$ mutants (Fig. 2A,B; supplementary material Fig. S2). Apoptosis, as indicated by cleaved caspase-3 immunostaining, was also more important in the multilayered lung epithelium of $Yy1^{flox/flox}$;$Shh^{+/Cre}$ specimens (Fig. 2C,D). At E14.5, apoptosis was increased in lung mesenchyme from mutants (supplementary material Fig. S2). Together, reduced epithelial proliferation and augmented apoptosis contribute to the abnormal lung structure in $Yy1^{flox/flox}$;$Shh^{+/Cre}$ mutants.

Altered lung patterning and cell differentiation in $Yy1^{flox/flox}$;$Shh^{+/Cre}$ mutants

To investigate whether the proximal-distal patterning of airway epithelium was disrupted in $Yy1^{flox/flox}$;$Shh^{+/Cre}$ mutants, we examined the expression of the transcription factors sex-determining region Y (SRY)-box 2 and 9 (SOX2 and SOX9), two lineage commitment markers of proximal and distal endodermal lung progenitor cells, respectively (Tian et al., 2011). In controls, SOX2 was expressed in the epithelium of trachea and proximal airways, whereas SOX9 was present in the epithelium of distal tubular tips and in the mesenchyme lining proximal airways. In mutants, SOX2 and SOX9 epithelial expression also displayed a reciprocal pattern, but SOX2 expression was downregulated and restricted to a more proximal region (Fig. 2E-H). We further characterized epithelial cell specification by examining the expression of NKX2-1 and FOXA2, two transcription factors essential for lung branching and epithelial cell differentiation (Kimura et al., 1996; Minoo et al., 1999; Wan et al., 2004). No major difference was observed (Fig. 2I-L).

In agreement with the lack of SOX2 expression along the cysts, no secretory club (Clara) cells or ciliated cells, normally found along the proximal airway epithelium, were detected in the cystic epithelium (Fig. 2M-P). In contrast, Types I and II pneumocytes were present along the cyst-lining epithelium (Fig. 2Q-X). Microvascular development, as detected by PECAM immunostaining, also occurred within the mesenchyme surrounding the cysts (Fig. 2Y,Z).

In E12.5 controls, expression of alpha smooth muscle actin (αSMA), a marker of airway smooth muscle differentiation, was detected in myofibroblasts surrounding blood vessels and conducting airways, but excluded from the tip of growing buds. In mutants, αSMA-positive cells were lacking around cysts, but still present around pulmonary vasculature (Fig. 2AA,BB). Thus, *Yy1* epithelial ablation prevents branching morphogenesis with no major consequences on the specification of the distal epithelium. However, it interferes with the differentiation or the survival of airway myofibroblasts.

Abnormal formation of cartilage rings and impaired cell differentiation in trachea from $Yy1^{flox/flox}$;$Shh^{+/Cre}$ mutants

The trachea from $Yy1^{flox/flox}$;$Shh^{+/Cre}$ mutants appeared thinner with disorganized cartilage rings (Fig. 1A-B). Alcian Blue staining verified the abnormal banding pattern (Fig. 3A,B). Tracheal stenosis was confirmed by the measurement of the external diameter (625 ±26 μm versus 339±25 μm; $P<0.001$) and the luminal surface area (61±16 μm^2 versus 4.6±2 μm^2; $P<0.01$), both of which were significantly smaller in mutants. The trachea was also longer in mutants (2029±130 μm versus 2487±47 μm; $P<0.01$) (Fig. 3A-E). We analyzed the expression of SOX9, a master regulator of chondrogenesis essential for tracheal cartilage patterning (Park et al., 2010). In E14.5 controls, the punctuated SOX9 expression pattern reflected future cartilage rings. Conversely, mutants displayed continuous SOX9 expression along the upper airways (Fig. 3F,G). Thus, epithelial YY1 controls the condensation of SOX9-positive mesenchymal cells into precartilage nodules.

We assessed the expression of p63, a marker of basal cells, which are known to generate ciliated, club and goblet cells (Rock et al., 2009). Basal cells were distributed irregularly along the proximal airways of $Yy1^{flox/flox}$;$Shh^{+/Cre}$ embryos (Fig. 3H,I). Although the number of p63-positive basal cells was not noticeably altered, ciliated, club and goblet cells were scarce in mutants (Fig. 3H-M). SOX2 is crucial for tracheal cartilage

Table 1. Ratios of genotypes in litters from crosses between $Yy1^{flox/+}$;$Shh^{+/Cre}$ and $Yy1^{flox/flox}$ mice

$Yy1^{flox/+}$;$Shh^{+/Cre}$×$Yy1^{flox/flox}$

			$Shh^{+/+}$		$Shh^{+/Cre}$	
Age	# litters	# pups	$Yy1^{flox/+}$	$Yy1^{flox/flox}$	$Yy1^{flox/+}$	$Yy1^{flox/flox}$
Expected (%)			(25)	(25)	(25)	(25)
E12.5	21	144	31 (21.5)	41 (28.5)	37 (25.7)	35 (24.3)
E14.5	7	54	19 (35.2)	6 (11.1)	15 (27.8)	14 (25.9)
E18.5	9	59	13 (22.1)	16 (27.1)	12 (20.3)	18 (30.5)
P21	13	74	26 (35.1)	21 (28.4)	27 (36.5)	0 (0)

The percentage obtained is indicated in parentheses.

Development (2015) 142, 2981-2995 doi:10.1242/dev.120469

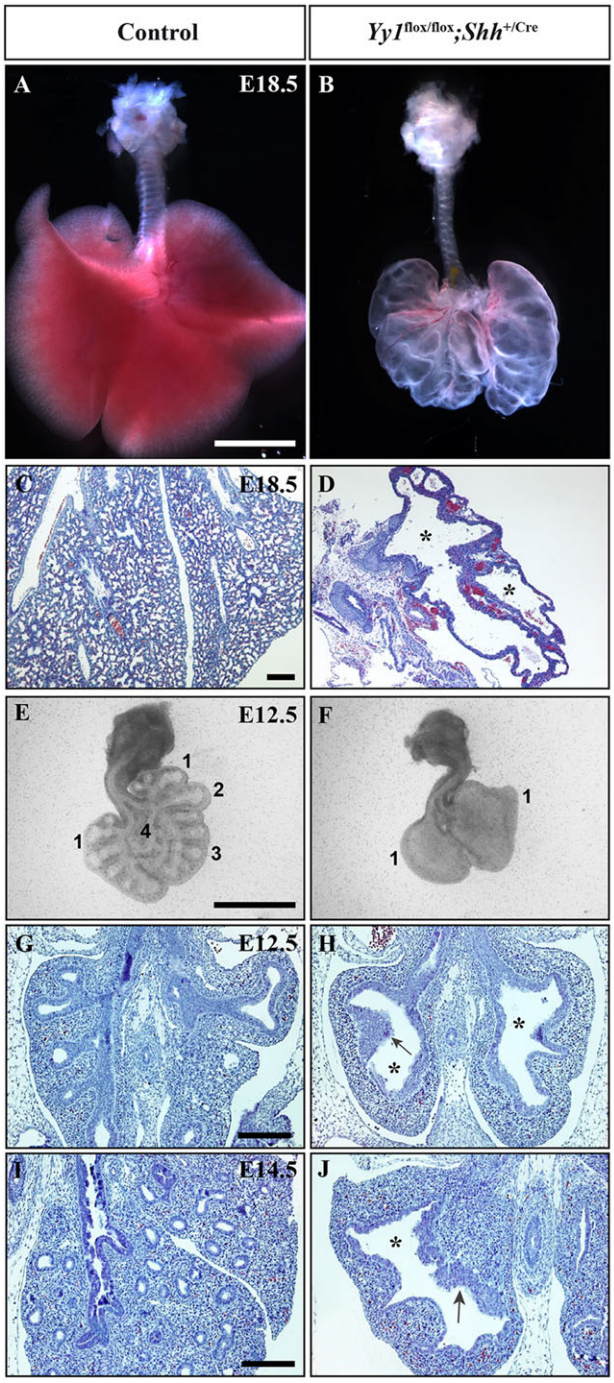

Fig. 1. *Yy1* is crucial for lung branching morphogenesis. (A,B) Lungs from E18.5 *Yy1*$^{flox/flox}$;*Shh*$^{+/Cre}$ embryos (B) showed dilated sacs instead of the well-formed lobes seen in controls (A). (C,D,G-J) H&E-stained lung sections revealed that as early as E12.5, *Yy1*$^{flox/flox}$;*Shh*$^{+/Cre}$ mutants displayed defective airway branching causing cyst formation (asterisks) with an abnormal stratified epithelium (arrows). (E,F) Whole-mount lungs from E12.5 control and *Yy1*$^{flox/flox}$;*Shh*$^{+/Cre}$ lungs presented left isomerism. Labels 1-4 represent lobes. Scale bars: 2 mm in A,B; 200 µm in C,D,G-J; 1 mm in E,F.

patterning and epithelial cell differentiation (Que et al., 2009). In controls, SOX2 was expressed in all airway epithelial cells. In mutants, SOX2 signal was unevenly spread along the tracheal epithelium, a result reminiscent of the abnormal SOX2 expression in lungs from E12.5 *Yy1*$^{flox/flox}$;*Shh*$^{+/Cre}$ embryos (Figs 2E,F and 3N,O). These data underscore the non-cell-autonomous role of YY1 in tracheal cartilage patterning and its cell-autonomous function in airway epithelial cell differentiation.

Yy1 epithelial inactivation affects the expression of key players of lung development

We assessed by qRT-PCR if the *Yy1* mutation caused the misregulation of molecules with established roles in lung morphogenesis. During branching, FGF10 is dynamically expressed in mesenchymal clustered cells, inducing the activation of the ERK/MAPK pathway in the adjacent epithelium to control the directional outgrowth of lung buds (Bellusci et al., 1997). At E14.5, *Fgf10* expression was 2.7-fold higher in *Yy1*$^{flox/flox}$;*Shh*$^{+/Cre}$ lungs compared with *Yy1*$^{flox/+}$;*Shh*$^{+/Cre}$ controls. Consequently, expression of *Bmp4*, *Spry2* and *Etv4* genes, known targets of lung FGF10 signaling, was upregulated in mutants (Fig. 4A; Weaver et al., 2000; Mailleux et al., 2001; Liu et al., 2003). Reduced expression of *Etv5*, another target of FGF10 signaling, was also observed. *In situ* hybridization assays revealed an expanded spatial distribution of *Fgf10* mRNA in lungs from E12.5 mutants (Fig. 4B,C). Accordingly, increased expression of phospho-ERK (pERK), the activated form of ERK, was observed in the cystic epithelium of *Yy1*$^{flox/flox}$;*Shh*$^{+/Cre}$ embryos (Fig. 4D,E). Expression of *Fgf9*, *Hoxa5*, *Hoxb5*, *Foxp1*, *Foxp2*, *Foxp4*, *Hdac1*, and *Hdac2* genes, all involved in lung branching, was also monitored (Aubin et al., 1997; White et al., 2006; Shu et al., 2007; Wang et al., 2011, 2013). With the exception of a reduction in expression of *Fgf9* and *Foxp2*, no change in gene expression was detected (Fig. 4A).

YY1 positively regulates *Shh* expression

Shh null mutants present rudimentary lung sacs and tracheal-bronchial cartilage defects that mirror the *Yy1*$^{flox/flox}$;*Shh*$^{+/Cre}$ phenotype. Moreover, increased *Fgf10* and *Bmp4* lung expression levels are common denominators in *Yy1* and *Shh* mutants. Finally, αSMA-positive cells are absent around the bronchi in *Shh*$^{-/-}$ mutants (Litingtung et al., 1998; Pepicelli et al., 1998; van Tuyl et al., 2007). We examined *Shh* expression in *Yy1* mutants. The *Shh*^{Cre} allele used to generate the *Yy1* epithelial deletion is a Cre knock-in producing a *Shh* null allele (Harfe et al., 2004). To eliminate any bias that might result from *Shh* haploinsufficiency, *Shh* expression levels were measured by qRT-PCR in lungs from E14.5 *Yy1*$^{flox/flox}$;*Shh*$^{+/Cre}$ mutants and compared to *Yy1*$^{+/flox}$;*Shh*$^{+/Cre}$ specimens. *Shh* expression, as well as that of *Ptc1*, *Hip1* and *Foxf1*, targets of the SHH pathway, was significantly decreased in *Yy1*$^{flox/flox}$;*Shh*$^{+/Cre}$ lungs (Fig. 4F; Pepicelli et al., 1998; Chuang and McMahon, 1999; Mahlapuu et al., 2001).

Shh expression is confined to lung epithelium, suggesting that *Shh* may be a direct target of YY1. Sequence comparison with TFSEARCH and TESS databases revealed putative YY1 binding sites clustered into five domains spread along the 4.5 kb upstream sequences relative to the transcription start site (TSS) of the *Shh* murine gene. To establish whether these sites were effective *in vivo*, we performed ChIP assay on cross-linked chromatin from lungs of E14.5 wild-type embryos. We observed high occupancy by YY1 of *Shh* upstream sequences and the *Tra2b* (also known as *Sfrs10*) positive control, and no binding with the *Rcor3* and *Shh* locus negative controls (Fig. 4G; Kang et al., 2009). Thus, YY1 can physically interact with *Shh* regulatory sequences *in vivo* during lung development. Using a transfection reporter assay in HEK293 cells, we demonstrated that YY1 activated transcription of the luciferase reporter gene placed under the control of 5 kb upstream sequences of the *Shh* murine gene (supplementary

Development (2015) 142, 2981-2995 doi:10.1242/dev.120469

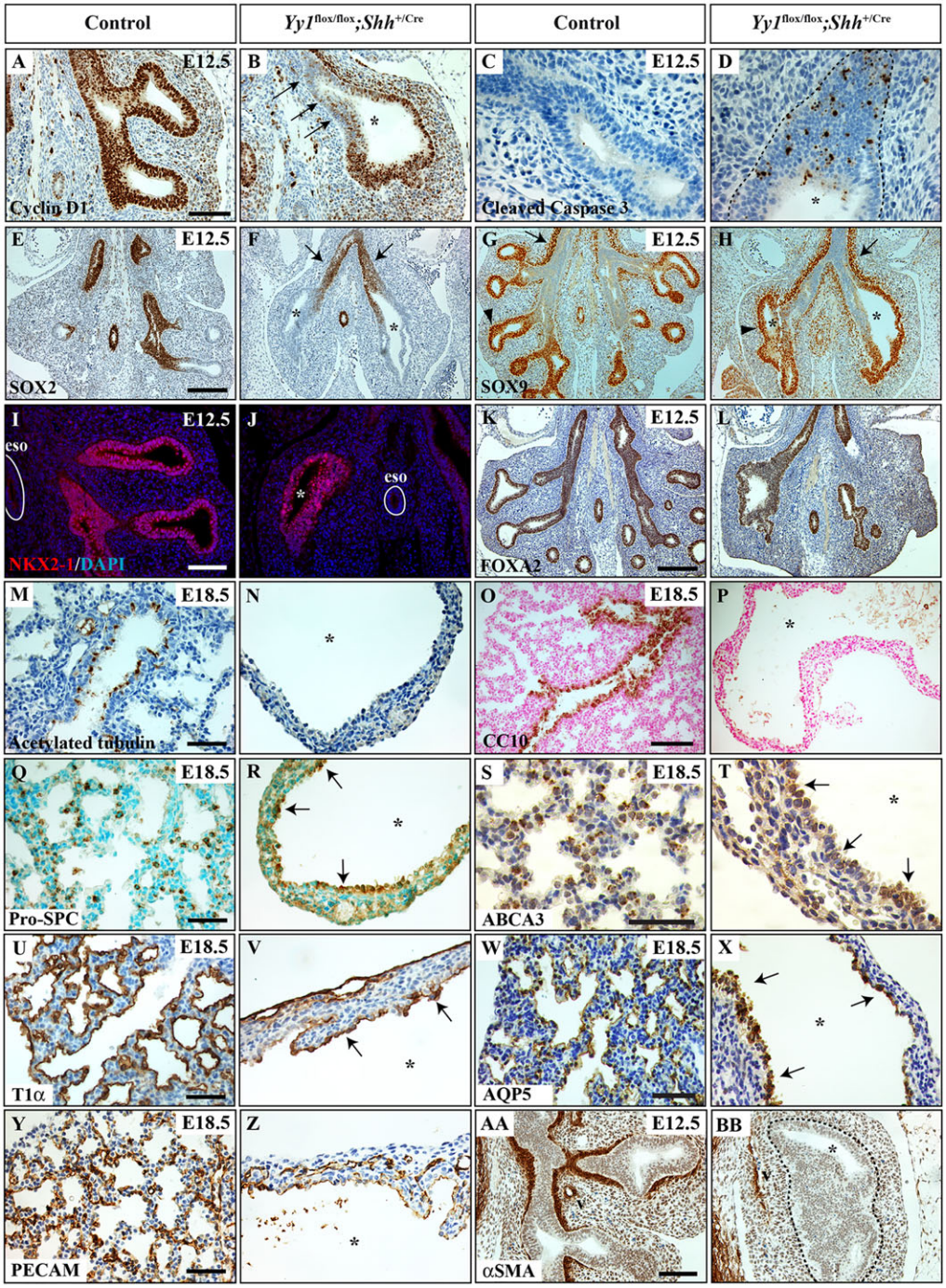

Fig. 2. YY1 controls lung epithelial proliferation and apoptosis, patterning and airway myofibroblast differentiation. (A,B) Reduced cyclin D1 epithelial immunostaining (arrows) revealed decreased cell proliferation in lung epithelium of E12.5 *Yy1*$^{flox/flox}$;*Shh*$^{+/Cre}$ embryos. (C,D) Cleaved caspase-3 immunostaining showed massive apoptosis in lung epithelium of mutants. (E-H) SOX2 (E,F) and SOX9 (G,H) immunostaining assays revealed that SOX2 and SOX9 displayed reciprocal epithelial expression patterns in the developing airways from E12.5 control and *Yy1*$^{flox/flox}$;*Shh*$^{+/Cre}$ embryos. In mutants, SOX2 expression was downregulated (arrows) and restricted to a more anterior territory. Arrowheads indicate SOX9 expression. (I-L) Lungs from E12.5 controls and *Yy1*$^{flox/flox}$;*Shh*$^{+/Cre}$ mutants demonstrated comparable NKX2-1 (I,J) and FOXA2 (K,L) expression in airway epithelium. (M-P) Neither ciliated nor club cells, as detected by IHC with acetylated tubulin (M,N) and CC10 (O,P) specific markers, respectively, were observed in cyst epithelium of E18.5 *Yy1*$^{flox/flox}$;*Shh*$^{+/Cre}$ mutants. (Q-X) Cysts were lined by Type II and Type I pneumocytes as revealed by proSP-C (Q,R), ABCA3 (S,T), and T1α (U,V) and AQP5 (W,X) specific markers, respectively (arrows). (Y,Z) A microvascular network detected by PECAM IHC was present in the parenchyma forming the cyst walls. (AA,BB) At E12.5, no αSMA expression was detected around the bronchi in *Yy1*$^{flox/flox}$;*Shh*$^{+/Cre}$ specimens. Asterisks indicate cysts. eso, esophagus; v, vasculature. Scale bars: 50 µm in C,D,M,N,Q-Z; 100 µm in A,B,I,J,O,P,AA,BB; 200 µm in E-H, K,L.

material Fig. S3). Taken together, these data support the notion that YY1 is a transcriptional activator of *Shh* expression in lung epithelium.

Yy1$^{flox/flox}$;*Tg*$^{Nkx2\text{-}1Cre}$ and *Yy1*$^{flox/flox}$;*Shh*$^{+/Cre}$ mice share lung phenotype characteristics

To inactivate *Yy1* in the developing lung endoderm in a *Shh* haploinsufficiency-independent context, we used the BAC-*Nkx2-1-Cre* transgenic deleter line (Xu et al., 2008). *Yy1*$^{flox/flox}$;*Tg*$^{+/Nkx2\text{-}1Cre}$ embryos exhibited cysts in the proximal region of the lobes, a phenotype consistent with the gradient of activity of the recombinase (Fig. 5A-I). As observed in *Yy1*$^{flox/flox}$;*Shh*$^{+/Cre}$ mutants, Types I and II pneumocytes, but not club and ciliated cells, were present along the cystic epithelium (supplementary material Fig. S4). Decreased *Shh* and *Hip1* and increased *Fgf10* expression levels were detected in lungs from *Yy1*$^{flox/flox}$;*Tg*$^{+/Nkx2\text{-}1Cre}$ embryos, providing additional evidence that epithelial YY1 regulates *Shh* expression (Fig. 5J).

SHH partially rescues the lung phenotype of *Yy1*$^{flox/flox}$;*Shh*$^{+/Cre}$ mutants

We tested whether addition of recombinant mouse SHH (rmSHH) could rescue the *Yy1* lung phenotype *in vitro*. Lungs from E12.5 *Yy1*$^{flox/flox}$;*Shh*$^{+/Cre}$ embryos cultured in control media failed with branch. They showed a loss of αSMA immunoreactivity around the cysts and an increased number of apoptotic cells when compared with controls (Fig. 6). Addition

Development (2015) 142, 2981-2995 doi:10.1242/dev.120469

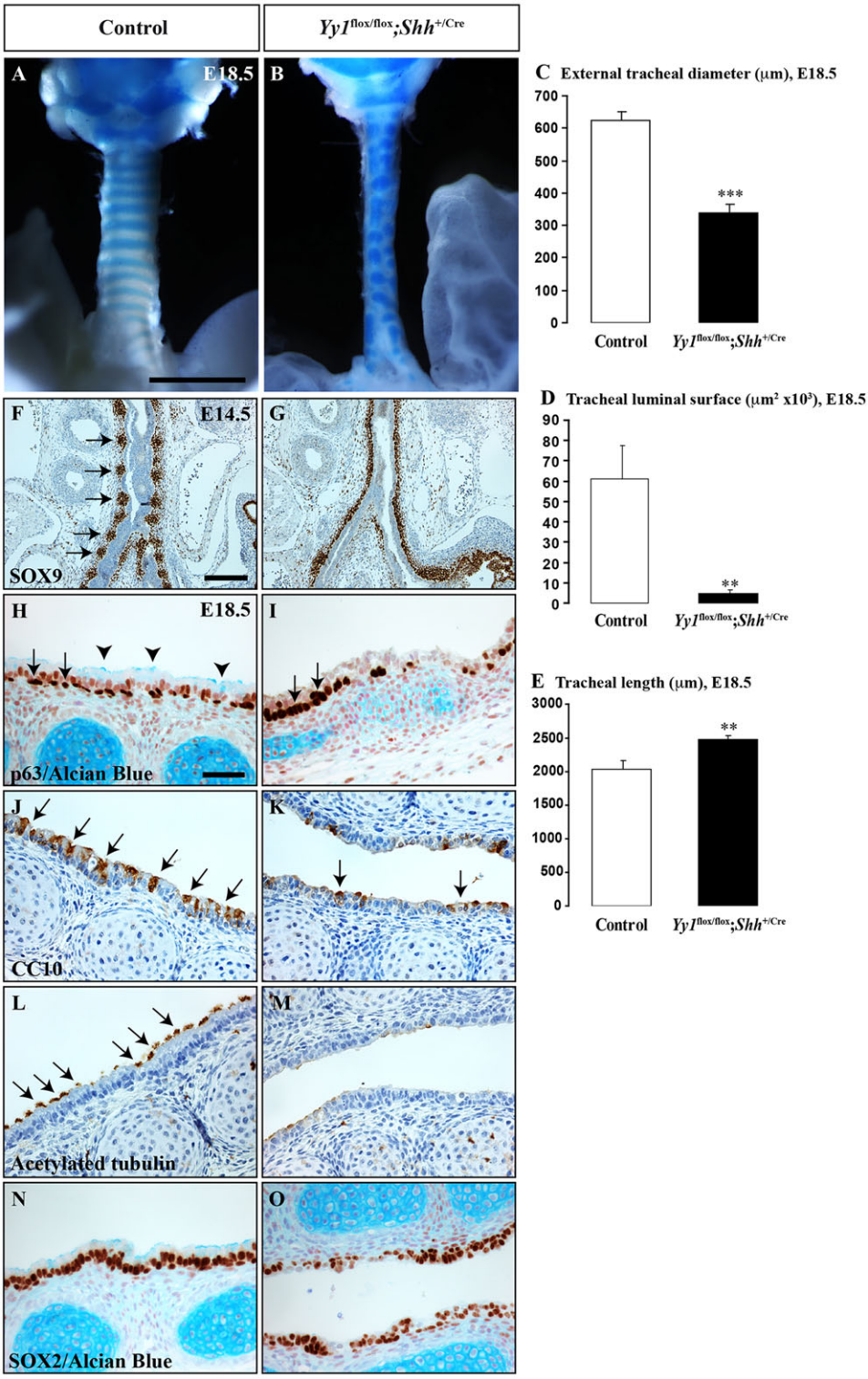

Fig. 3. Abnormal cartilage ring patterning and epithelial cell differentiation in the trachea of *Yy1*$^{flox/flox}$;*Shh*$^{+/Cre}$ embryos. (A,B) As shown by Alcian Blue staining, the C-shaped cartilaginous rings, segmentally distributed along the trachea in controls, were replaced by irregular patches of cartilage in E18.5 *Yy1*$^{flox/flox}$;*Shh*$^{+/Cre}$ embryos. (C-E) Reduced external tracheal diameter and luminal surface, and increased tracheal length were observed in E18.5 *Yy1*$^{flox/flox}$;*Shh*$^{+/Cre}$ mutants. Values are expressed as mean±s.d.; $^{**}P<0.01$, $^{***}P<0.001$; n=3-4/genotype. (F,G) Unsegmented SOX9 expression was observed along the upper airways of E14.5 *Yy1*$^{flox/flox}$;*Shh*$^{+/Cre}$ embryos when compared with controls. Arrows indicate punctuated SOX9 expression. (H-M) p63 (H,I), CC10 (J,K) and acetylated tubulin (L,M) immunostaining assays detected basal, club and ciliated cells, respectively (arrows). Mucus-producing goblet cells were detected with Alcian Blue (arrowheads, H-I). In mutants, basal cells were irregularly distributed along the proximal airways and a near-complete loss of club, goblet and ciliated cells was observed. (N,O) SOX2-positive cells were less abundant and more dispersed along the tracheal epithelium of mutants. Scale bars: 1 mm in A,B; 200 μm in F,G; 50 μm in H-O.

of rmSHH to *Yy1*$^{flox/+}$;*Shh*$^{+/Cre}$ explants caused an increased overall size, probably due to the thickened mesenchymal layer (Fig. 6C,D). The rmSHH treatment of *Yy1*$^{flox/flox}$;*Shh*$^{+/Cre}$ explants did not rescue the branching defect (Fig. 6G,H). However, apoptosis in rmSHH-supplemented *Yy1*$^{flox/flox}$;*Shh*$^{+/Cre}$ lungs returned to control levels (Fig. 6M-P). Moreover, αSMA expression at the periphery of cysts was partially recovered, corroborating the importance of SHH in airway smooth muscle cell specification (Fig. 6I-L).

Decreased YY1 expression in PPB lung specimens

The presence of lung cysts in *Yy1*$^{flox/flox}$;*Shh*$^{+/Cre}$ and *Yy1*$^{flox/flox}$;*Tg*$^{+/Nkx2\text{-}1Cre}$ mutants mimics features of CCAM and PPB, two human pediatric cystic lung diseases (Stocker, 2009). To define the clinical relevance of our findings, YY1 immunostaining was performed on lung sections from children suffering from types I and II CCAM, and types I, II and III PPB and compared with lung specimens from age-matched patients who died from a non-pulmonary cause (supplementary material Table S1). PPB evolves

Development (2015) 142, 2981-2995 doi:10.1242/dev.120469

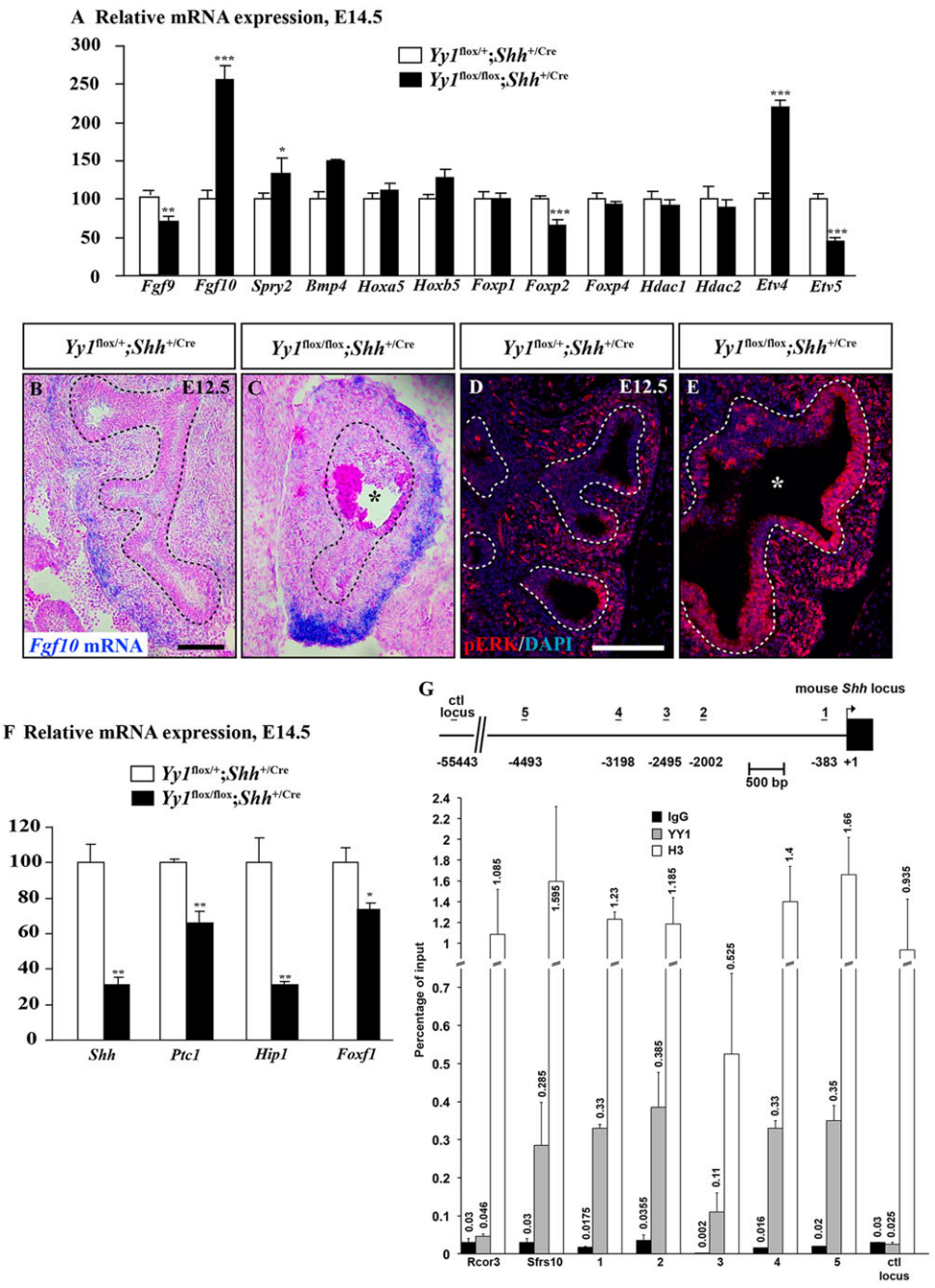

Fig. 4. Epithelial *Yy1* inactivation affects *Fgf10* and *Shh* expression. (A) qRT-PCR expression analysis revealed increased levels of *Fgf10*, *Spry2* and *Etv4* and decreased levels of *Fgf9*, *Foxp2* and *Etv5* in lungs from E14.5 $Yy1^{flox/flox}$;$Shh^{+/Cre}$ embryos when compared with $Yy1^{flox/+}$;$Shh^{+/Cre}$ specimens. Values are expressed as mean±s.e.m.; **P*<0.05, ***P*<0.01, ****P*<0.001. (B,C) Increased *Fgf10* expression was detected by *in situ* hybridization in lung mesenchyme surrounding the dilated airways of E12.5 $Yy1^{flox/flox}$;$Shh^{+/Cre}$ embryos. (D,E) Phospho-ERK (pERK) expression was stronger and more abundant in the cyst epithelium in E12.5 mutants, reflecting the increased FGF10 signaling activity. (F) qRT-PCR analyses showed the reduced expression of *Shh* and its target genes *Ptc1*, *Hip1* and *Foxf1* in lungs from E14.5 $Yy1^{flox/flox}$;$Shh^{+/Cre}$ mutants. Values are expressed as mean±s.e.m.; **P*<0.05, ***P*<0.01. (G) Upper panel: schematic representation and position relative to the TSS of the five putative YY1 binding sites in the *Shh* promoter. The position of the qPCR fragments is indicated. Lower panel: ChIP analysis of endogenous *Shh* regulatory sequences in E14.5 lung. Chromatin was immunoprecipitated with rabbit IgG, anti-YY1 and anti-histone H3 antibodies. Recruitment of YY1 and H3 on regulatory sequences of the *Shh* locus was evaluated by qPCR and indicated as the percentage of input. YY1 bound to the *Shh* genomic regions spanning the YY1 binding sites whereas no binding was observed with the *Shh* negative control. The data indicated correspond to mean±s.d. of two independent experiments. Asterisks indicate cysts. Dashed lines indicate the demarcation between the airway epithelium and the mesenchyme. Scale bars: 100 µm in B,C; 200 µm in D,E.

through sequential pathological changes; the early stage (Type I) is characterized by a pure cystic architecture that progresses over time into a mixed cystic and solid lesion (Type II), which further evolves into a purely solid aggressive tumor with anaplastic undifferentiated sarcomatous components (Type III; Messinger et al., 2015). In controls and CCAM specimens, YY1 protein was strongly expressed in lung epithelium and mesenchyme. In specimens from all three types of PPB, YY1 staining was reduced, as assessed by IHC semiquantitative scoring (Fig. 7). These findings suggest a pathogenic role for YY1 in PPB.

No genetic interplay between *Yy1* and *Dicer* genes in lung morphogenesis

PPB is an extremely rare lung sarcoma that arises during fetal lung development and occurs in young children. PPB is associated with germ line and somatic mutations in the *DICER1* gene (Hill et al., 2009; Pugh et al., 2014). In mice, the conditional loss of *Dicer* function in lung epithelium causes neonatal death due to defective lung branching and airway dilation, similar to the phenotype of $Yy1^{flox/flox}$;$Shh^{+/Cre}$ mutants (Fig. 8A-D; Harris et al., 2006). These resemblances raised questions about a potential interplay between *Yy1* and *Dicer* genes in lung morphogenesis. We assessed *Dicer* expression levels between lungs from E14.5 $Yy1^{flox/+}$;$Shh^{+/Cre}$ and $Yy1^{flox/flox}$;$Shh^{+/Cre}$ embryos. No significant difference was found, indicating that YY1 did not control *Dicer* expression during lung formation (Fig. 8E). Likewise, a *Dicer* epithelial mutation did not perturb *Yy1* lung expression in $Dicer^{flox/flox}$;$Shh^{+/Cre}$ mutants at the RNA and protein levels (Fig. 8F; not shown).

As reported, the *Dicer* mutation caused increased *Fgf10* expression (*P*<0.001) (Fig. 8F; Harris et al., 2006). We also found

Development (2015) 142, 2981-2995 doi:10.1242/dev.120469

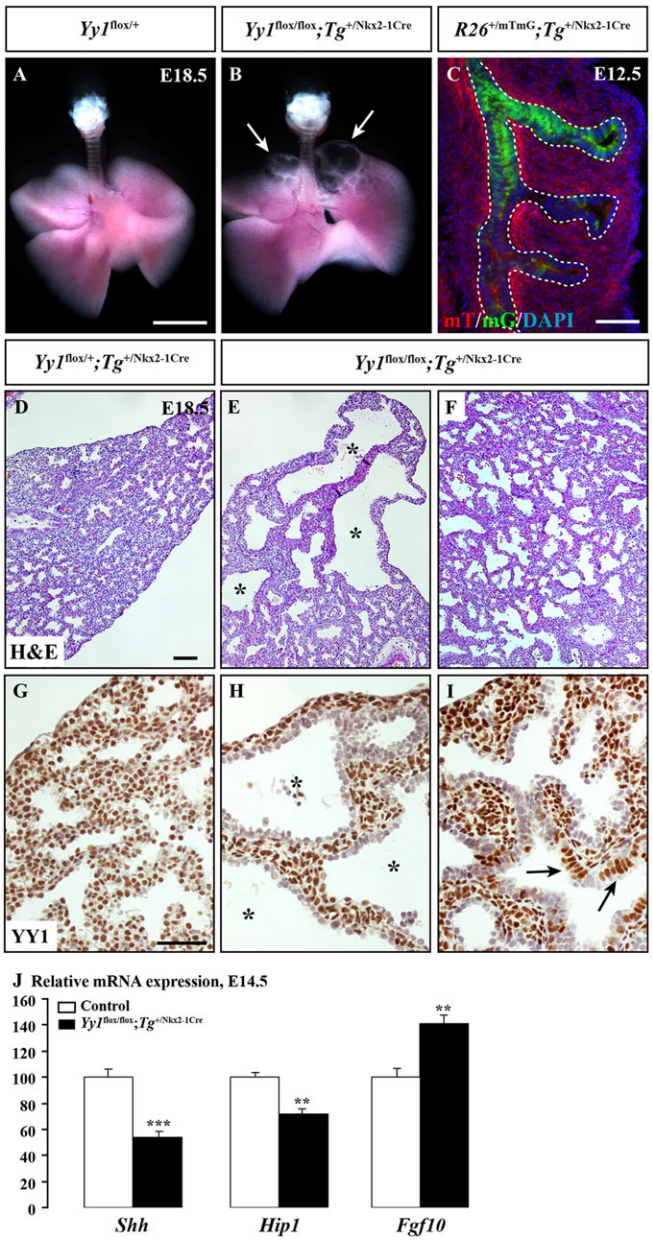

Fig. 5. *Yy1* inactivation in the developing lung endoderm with the *Nkx2-1Cre* transgenic mouse line causes cyst formation. (A,B) Lungs from E18.5 *Yy1*$^{flox/flox}$;*Tg*$^{+/Nkx2\text{-}1Cre}$ embryos exhibited cysts in the proximal region of the lobes (arrows). (C) A robust Cre activity was detected in the proximal respiratory epithelium from E12.5 *R26*$^{+/mTmG}$;*Tg*$^{+/Nkx2\text{-}1Cre}$ embryos. (D-F) H&E-stained lung sections revealed that E18.5 *Yy1*$^{flox/flox}$;*Tg*$^{+/Nkx2\text{-}1Cre}$ mutants presented defective airway branching as shown by the formation of cysts (asterisks). Panels E and F correspond to the proximal and distal parts of the lung, respectively. (G-I) YY1 immunostaining demonstrated a near-complete loss of YY1 expression in the epithelium lining cysts in the proximal portion of the lungs from E18.5 *Yy1*$^{flox/flox}$;*Tg*$^{+/Nkx2\text{-}1Cre}$ mutants (H). The deletion was incomplete in distal lung as shown by YY1-positive cells (arrows; I). (J) qRT-PCR analysis revealed decreased *Shh* and *Hip1* expression and increased *Fgf10* levels in lungs from E14.5 *Yy1*$^{flox/flox}$; *Tg*$^{+/Nkx2\text{-}1Cre}$ embryos. Values are expressed as mean±s.e.m.; $^{**}P<0.01$, $^{***}P<0.001$. Asterisks indicate cysts. Scale bars: 2 mm in A,B; 100 µm in C-F; 50 µm in G-I.

reduced expression of *Shh* ($P<0.01$) and its targets *Ptc1* ($P<0.01$) and *Hip1* ($P<0.05$) in *Dicer*$^{flox/flox}$;*Shh*$^{+/Cre}$ specimens compared with *Dicer*$^{flox/+}$;*Shh*$^{+/Cre}$ controls (Fig. 8F). Therefore, both *Yy1* and *Dicer* genes regulate *Shh* expression and subsequent lung branching morphogenesis.

To address if genetic interactions occur between the *Yy1* and *Dicer* genes *in vivo*, we generated *Yy1*$^{flox/+}$;*Dicer*$^{flox/+}$;*Shh*$^{+/Cre}$ double heterozygous animals. Like single heterozygous mutants, *Yy1*$^{flox/+}$;*Dicer*$^{flox/+}$;*Shh*$^{+/Cre}$ embryos did not present lung defects, suggesting no genetic interplay (not shown). Accordingly, *Shh* expression levels were similar in lungs from single and double heterozygous mutants and comparable to that detected in *Shh*$^{+/Cre}$ specimens (Fig. 8G). Thus, the homozygous mutation of either *Yy1* or *Dicer* in lung epithelium is required to significantly reduce *Shh* expression.

Microarray analysis of RNA from lungs of E14.5 *Shh*$^{+/Cre}$, *Yy1*$^{flox/flox}$;*Shh*$^{+/Cre}$ and *Dicer*$^{flox/flox}$;*Shh*$^{+/Cre}$ embryos was performed to assess the molecular consequences of the *Yy1* and *Dicer* mutations in lung epithelium (supplementary material Fig. S5). An analysis of the total number of differentially expressed genes with a fold change ≥1.5 and $P<0.05$ revealed an overlap of 210 genes of which only seven were regulated in opposite direction. This suggested that a core pattern of altered gene expression is associated with airway dilation common to the two models. A heat map was established. In addition to confirming the modified expression of *Shh*, *Hip1* and *Fgf10* genes, it revealed the upregulation of *Cdkn1a*, known to be repressed by YY1 (Affar et al., 2006). *Cdkn1a* encodes the cyclin-dependent kinase inhibitor p21, and its upregulation concurred with the reduced proliferation observed in mutants. The detected decrease in expression of *Elf5*, *Irx2*, *Irx3* and *Irx5* genes, encoding transcriptional regulators of lung morphogenesis, also corroborates the observed lung phenotype. Inhibition of *Irx* expression has been shown to cause reduced lung branching (van Tuyl et al., 2006). *Elf5* misexpression in lung epithelium also disrupts branching, suggesting that precise levels of *Elf5* are required for lung morphogenesis (Metzger et al., 2008).

Yy1$^{flox/flox}$;*Tg*$^{Nkx2\text{-}1Cre}$ mice present a PPB-like phenotype

The neonatal lethality of *Yy1*$^{flox/flox}$;*Shh*$^{+/Cre}$ mice precluded the study of lung tumor formation and progression. However, proliferation assays in lungs from E18.5 *Yy1*$^{flox/flox}$;*Shh*$^{+/Cre}$ and *Dicer*$^{flox/flox}$;*Shh*$^{+/Cre}$ embryos revealed a dramatic increase in cell proliferation of the cystic walls, suggesting tissue overgrowth (Fig. 9A-D).

The lung phenotype of *Yy1*$^{flox/flox}$;*Tg*$^{+/Nkx2\text{-}1Cre}$ embryos was less severe than the *Yy1*$^{flox/flox}$;*Shh*$^{+/Cre}$ phenotype. However, increased proliferation was also detected in lungs from E18.5 *Yy1*$^{flox/flox}$;*Tg*$^{+/Nkx2\text{-}1Cre}$ embryos (supplementary material Fig. S4K,L). Most *Yy1*$^{flox/flox}$;*Tg*$^{+/Nkx2\text{-}1Cre}$ mutants died at birth but some survived up to weaning age (Table 2). Out of 86 pups, seven *Yy1*$^{flox/flox}$;*Tg*$^{+/Nkx2\text{-}1Cre}$ mice born alive survived until weaning or were sacrificed due to health problems. The lungs of these seven mice exhibited cysts in the proximal region and histological analyses showed a multiloculated structure with septa of variable thicknesses around cysts (Fig. 9E-G). Elevated proliferation was observed in the disorganized mass (Fig. 9I,J). Vimentin immunostaining confirmed the mesenchymal nature of the tissue (Fig. 9K,L). Putative primitive small mesenchymal cells, a hallmark of type I PPB, were also detected (Fig. 9H). Finally, NKX2-1 and T1α positive cells revealed the alveolar nature of the cyst epithelium (Fig. 9O,P). Altogether, these characteristics are reminiscent of the histologic features of an evolving type I PPB (Hill et al., 2008).

Development (2015) 142, 2981-2995 doi:10.1242/dev.120469

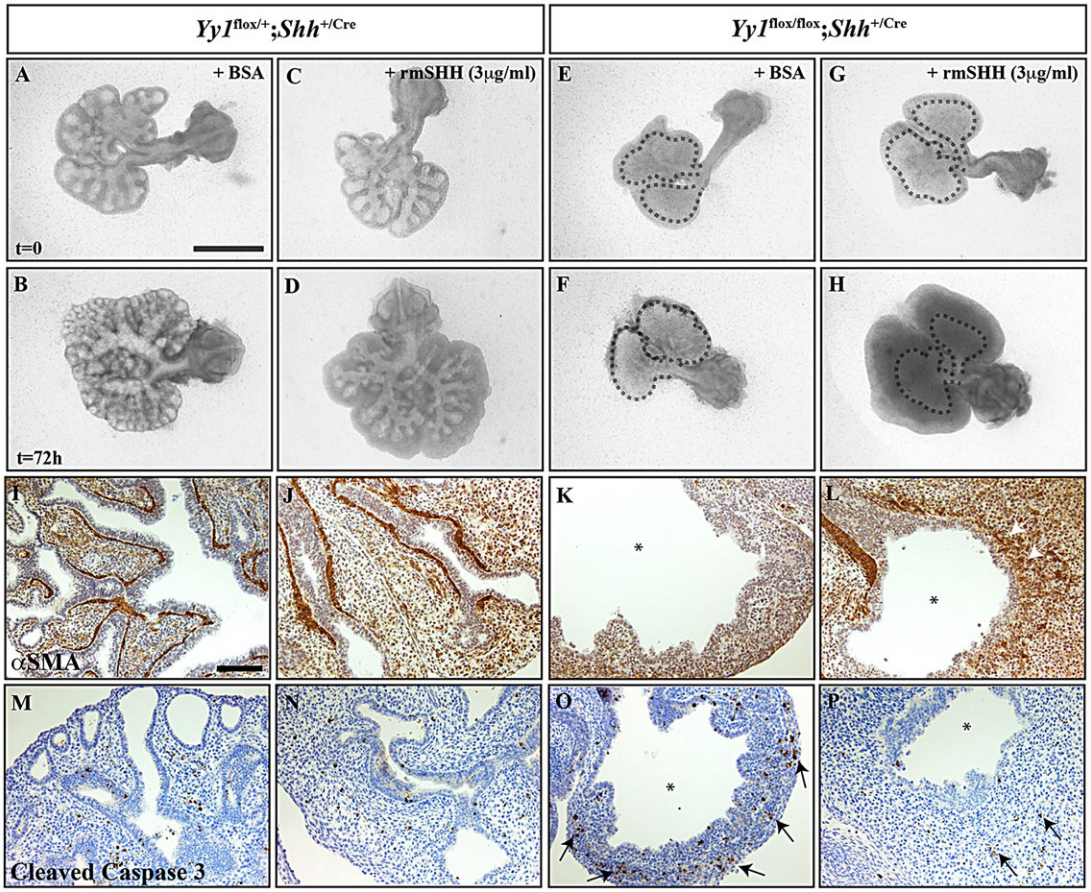

Fig. 6. Addition of rmSHH partially rescues the airway smooth muscle cells and the apoptotic defects in *Yy1*$^{flox/flox}$;*Shh*$^{+/Cre}$ lung explants. Lung explants from E12.5 *Yy1*$^{flox/+}$;*Shh*$^{+/Cre}$ (A-D,I,J,M,N) and *Yy1*$^{flox/flox}$;*Shh*$^{+/Cre}$ (E-H,K,L,O,P) embryos were cultured for 3 days with (C,D,G,H,J,L,N,P) or without (A,B,E,F,I,K,M,O) rmSHH. BSA-treated *Yy1*$^{flox/flox}$;*Shh*$^{+/Cre}$ explants exhibited cysts and failed to branch (E,F). They showed a loss of αSMA immunoreactivity around the cysts (I,K) and an increased number of apoptotic cells (M,O). Addition of rmSHH caused an increased size of the mesenchymal layer in both *Yy1*$^{flox/+}$;*Shh*$^{+/Cre}$ and *Yy1*$^{flox/flox}$;*Shh*$^{+/Cre}$ explants but did not improve lung branching in mutants (C,D,G,H). rmSHH partially restored αSMA expression in *Yy1*$^{flox/flox}$;*Shh*$^{+/Cre}$ explants (I-L). The number of apoptotic cells in *Yy1*$^{flox/flox}$;*Shh*$^{+/Cre}$ lungs supplemented with rmSHH returned to control levels (M-P). Arrows indicate cleaved caspase 3-positive cells. Asterisks indicate cysts, which are delineated by a dashed line. (*n*=3-5 per condition). Scale bars: 1 mm in A-H; 100 µm in I-P.

DISCUSSION

YY1 is a multifunctional transcription factor member of the Polycomb group protein family, and its actions are controlled by protein-protein interactions (Gordon et al., 2006). YY1 plays pivotal roles throughout development. In the lung, there is a dosage-dependent requirement for YY1 with a lower limit of expression for survival as hypomorph mutants die at birth from respiratory distress due to collapsed lungs (Affar et al., 2006). This phenotype was reproduced when we specifically ablated *Yy1* function in the mesenchyme. Moreover, *Yy1* lung mesenchymal deletion affects epithelial cell differentiation indicating an YY1 non-cell autonomous role (Bérubé-Simard et al., 2014). Here, we demonstrated that the *Yy1* mutation in lung epithelium also impacts on lung formation. *Yy1* function is thus required in both mesenchymal and epithelial cell layers for the correct development of the respiratory tract.

Epithelial inactivation of the *Yy1* gene inhibited lung branching but maintained distal epithelial cell differentiation, which agrees with the notion of negative correlation between branching and alveolar differentiation (Chang et al., 2013). The *Yy1* mutation also caused the formation of large cysts that mimicked the *Shh* lung phenotype (Litingtung et al., 1998; Pepicelli et al., 1998). *Shh* expression was decreased in *Yy1* mutant lungs independently of the *Cre* allele used. SHH, a diffusible factor secreted by the lung epithelium, inhibits *Fgf10* expression in lung mesoderm (Bellusci et al., 1997). Consequently, *Fgf10* expression was upregulated in *Yy1* mutants, resulting in the loss of *Fgf10*-expressing foci in lung mesenchyme that normally trigger branching events. Gain in *Fgf10* expression may generate a driving force favoring the cystic dilation of airways in *Yy1* mutants (Fig. 10). This mechanistic explanation is further supported by the observations that trans-uterine intraparenchymal microinjections of a vector carrying an *Fgf10* transgene induce cystic lung malformations in rat fetuses that recapitulate the phenotype of human congenital cystic lung diseases (Gonzaga et al., 2008). Therefore, our work uncovers a functional cascade sequentially implicating *Yy1*, *Shh* and *Fgf10* genes in lung branching coordination.

One *Shh* wild-type allele remains in *Yy1*$^{flox/flox}$;*Shh*$^{+/Cre}$ specimens, raising concerns about the impact of *Shh* haploinsufficiency on the lung phenotype. We have shown that: (1) *Yy1*$^{+/flox}$;*Shh*$^{+/Cre}$ specimens did not present lung anomalies; (2) *Shh* expression was reduced in *Yy1*$^{flox/flox}$;*Shh*$^{+/Cre}$ specimens compared with *Yy1*$^{flox/+}$;*Shh*$^{+/Cre}$ samples; and (3) *Yy1*$^{flox/flox}$;*Tg*$^{+/Nkx2\text{-}1Cre}$ and *Yy1*$^{flox/flox}$;*Shh*$^{+/Cre}$ mutants share a similar lung phenotype. Moreover, *Shh*$^{+/-}$ mutants do not present lung anomalies and variations in *Fgf10* expression (van Tuyl et al., 2007). These data provide concordant evidence for a role of YY1 in the regulation of *Shh* expression in the lung

Development (2015) 142, 2981-2995 doi:10.1242/dev.120469

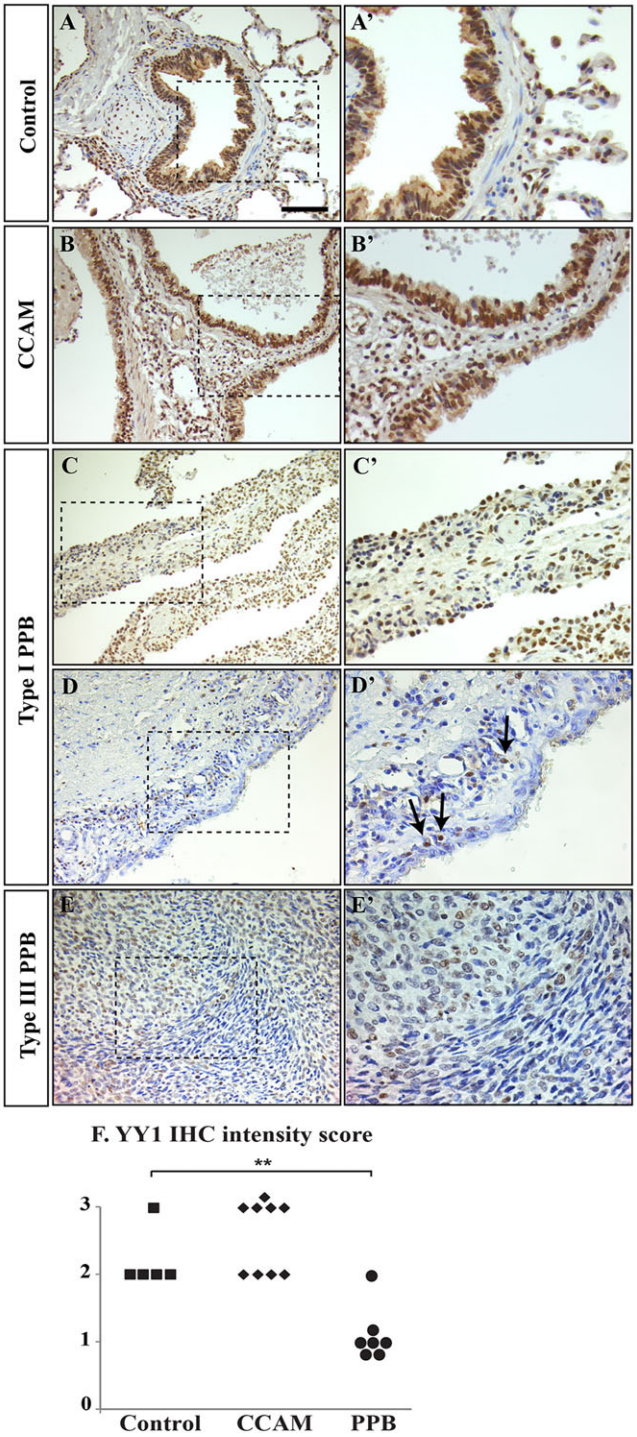

Fig. 7. YY1 expression in congenital cystic lung diseases. YY1 protein expression in lungs from control patients (A) or suffering from type I CCAM (B), type I PPB (C,D) and type III PPB (E). (F) The extent of YY1 staining was assessed by IHC semiquantitative scoring. Staining intensity was graded as 0 (negative), 1 (weak), 2 (moderate) and 3 (strong). Each symbol represents an individual specimen. Strong YY1 expression was observed in epithelial and mesenchymal cells from control and CCAM specimens, whereas less YY1-positive cells were detected in PPB specimens (arrows in D′). The boxed regions in A-E are magnified in A′-E′. Scale bar: 100 µm.

endoderm. ChIP data on the capacity of YY1 to directly bind *Shh* upstream regulatory sequences *in vivo* and transactivation assays in cell cultures reinforce the notion that YY1 acts as a direct transcriptional regulator of *Shh* expression in lung endoderm and alleviate the potential effect of the *Shh* heterozygous status on the phenotype observed.

The left pulmonary isomerism, the peribronchial smooth muscle differentiation defect and the tracheal–bronchial ring anomalies encountered in $Yy1^{flox/flox}$;$Shh^{+/Cre}$ specimens further support a role for YY1 in the positive regulation of *Shh* expression in the respiratory tract epithelium as these anomalies were also reported in *Shh* null mutants (Pepicelli et al., 1998; Tsukui et al., 1999). The tracheoesophageal fistula observed in *Shh* mutants was not reproduced in $Yy1^{flox/flox}$;$Shh^{+/Cre}$ mutants, probably due to the remaining low levels of *Shh* expression, suggesting that different SHH thresholds define specific SHH functions during respiratory tract development.

In the trachea, epithelial YY1 plays a non-cell autonomous role in the formation of the cartilage rings, whereas it acts directly on epithelial cell differentiation. In the distal lung, the *Yy1* epithelial mutation does not affect the specification of the epithelial cell types but it interferes with the specification of the airway smooth muscle cells. Addition of rmSHH to *Yy1* mutant lung explants can rescue the defective specification of αSMA-positive myofibroblasts and control apoptosis levels, strengthening the importance of SHH in mediating the non-cell autonomous role of epithelial YY1 in lung mesenchyme. However, the lack of branching of $Yy1^{flox/flox}$;$Shh^{+/Cre}$ explants in presence of rmSHH indicated that SHH is not the sole player in the *Yy1* lung phenotype. This is further supported by the microarray data revealing that several transcriptional regulators of lung development were differentially expressed in $Yy1^{flox/flox}$;$Shh^{+/Cre}$ specimens.

Formation of cystic-like structures is a characteristic of several mutations targeted to lung epithelium in mice. The epithelial inactivation of *Dicer* function with the Shh^{Cre} allele caused similar lung defects to those seen in $Yy1^{flox/flox}$;$Shh^{+/Cre}$ mice (Harris et al., 2006). Moreover, reduced *Shh* expression and augmented *Fgf10* expression occurred in $Dicer^{flox/flox}$;$Shh^{+/Cre}$ lung specimens, reinforcing the idea that dysregulated SHH-FGF10 signaling acts as a convergent point that induces events leading to cystic lung malformations.

Increased *Fgf10* expression appears to be a common denominator in the formation of lung cysts (Gonzaga et al., 2008). However, the reduced expression of *Etv5* and *Elf5* genes, encoding two transcription factors of the lung epithelium known to be under the positive control of FGF10, indicates that *Yy1* acts also on gene expression independently of FGF10 signaling (Liu et al., 2003; Metzger et al., 2007).

Addition of FGF9, another FGF important for lung development, to lung explant cultures also causes cyst-like structures (del Moral et al., 2006). *Fgf9* overexpression in lung epithelium induces epithelial branching arrest and luminal dilation in combination with decreased and increased *Shh* and *Fgf10* expression, respectively (White et al., 2006). Recently, augmented *Fgf9* expression was reported in the lung epithelium of E12.5 $Dicer^{flox/flox}$;$Shh^{+/Cre}$ embryos and type I PPB patients, whereas the $Dicer^{flox/flox}$;$Shh^{+/Cre}$ lung phenotype was attenuated by reduced *Fgf9* epithelial gene dosage (Yin et al., 2015). Our results indicated that *Fgf9* expression was not affected in lungs from E14.5 *Dicer* mutants, whereas it was reduced in *Yy1* mutant specimens. As *Fgf9* is expressed in both lung mesothelium and epithelium, a possibility remains that local variations in distinct cell populations, not detectable by a qRT-PCR global approach, may occur (Yin et al., 2011). Alternatively, variations in temporal *Fgf9* expression in *Dicer* mutant lungs might explain the differences.

Development (2015) 142, 2981-2995 doi:10.1242/dev.120469

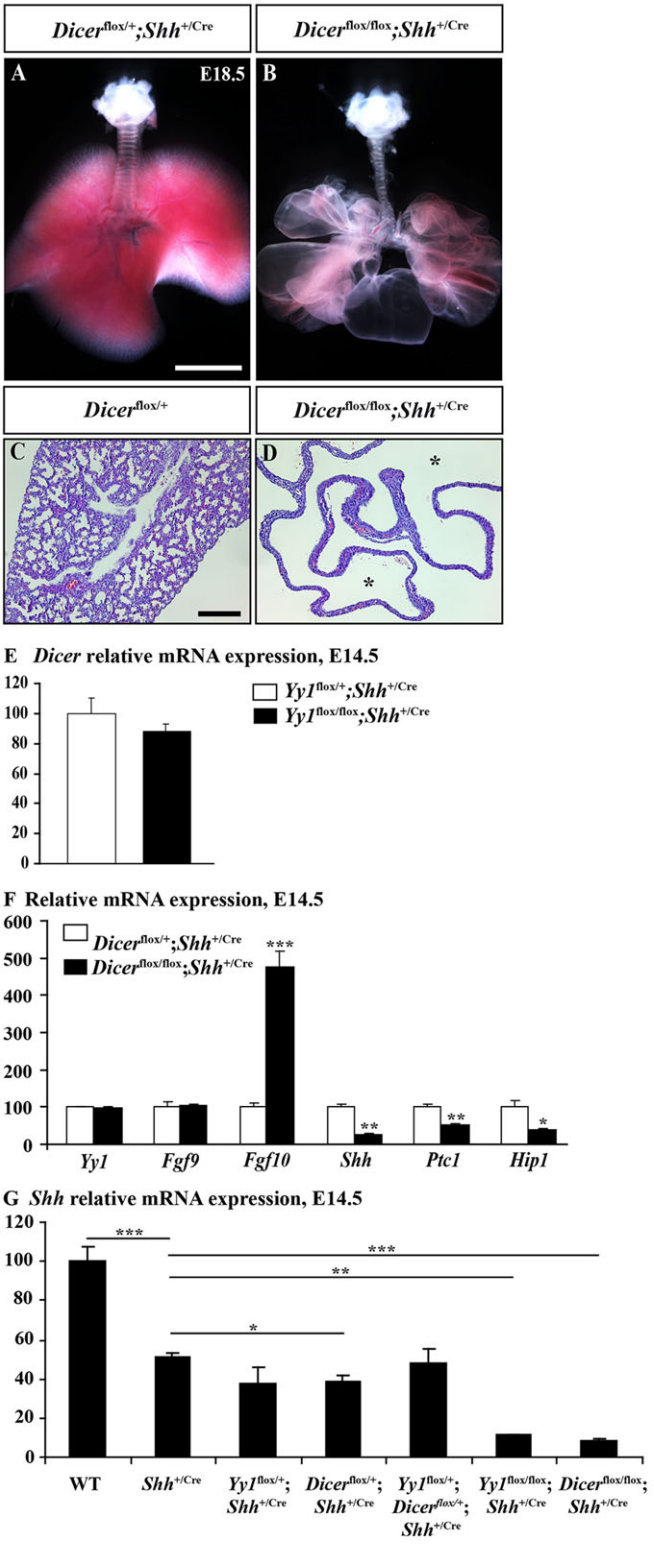

Fig. 8. Loss of *Dicer* function in the developing lung epithelium phenocopies the lung defects of *Yy1* mutants. (A,B) Lung from E18.5 *Dicer*$^{flox/flox}$;*Shh*$^{+/Cre}$ embryos showed dilated sacs. (C,D) H&E-stained lung sections revealed that lungs from E18.5 *Dicer*$^{flox/flox}$;*Shh*$^{+/Cre}$ mutants exhibited defects in airway branching causing cyst formation (asterisks). (E) *Dicer* expression was unchanged in lungs from E14.5 *Yy1*$^{flox/flox}$;*Shh*$^{+/Cre}$ embryos, as detected by qRT-PCR. (F) qRT-PCR analysis revealed increased levels of *Fgf10* expression and reduced expression levels for *Shh*, *Ptc1*, and *Hip1* in the lungs of E14.5 *Dicer*$^{flox/flox}$;*Shh*$^{+/Cre}$ embryos when compared with *Dicer*$^{flox/+}$;*Shh*$^{+/Cre}$ specimens. (G) Comparative analysis of *Shh* expression levels in lungs from E14.5 *Yy1*;*Dicer*;*Shh*$^{+/Cre}$ mutant embryos. *Shh* expression levels in single and double heterozygous mutants were comparable to that of *Shh*$^{+/Cre}$ specimens corresponding to ~40-50% of the levels in wild-type (WT) controls. In *Yy1*$^{flox/flox}$;*Shh*$^{+/Cre}$ embryos and *Dicer*$^{flox/flox}$;*Shh*$^{+/Cre}$ embryos, *Shh* expression levels were ~10% of that of WT specimens. (E-G) Values are expressed as mean±s.e.m.; **P*<0.05, ***P*<0.01, ****P*<0.001. Scale bars: 2 mm in A,B; 200 µm in C,D.

Despite the resemblances between *Yy1*$^{flox/flox}$;*Shh*$^{+/Cre}$ and *Dicer*$^{flox/flox}$;*Shh*$^{+/Cre}$ mutant lung phenotypes and the important overlap in differentially expressed lung genes, production of *Yy*$^{flox/+}$;*Dicer*$^{flox/+}$;*Shh*$^{+/Cre}$ double heterozygous mice and expression analyses did not provide evidence for a genetic interaction between *Yy1* and *Dicer* genes during lung morphogenesis. Therefore, *Dicer* and *Yy1* may act via distinct pathways to control lung development.

Although our data pointed toward a direct transcriptional regulation of *Shh* expression by YY1, the mechanisms of DICER action in lung epithelium remain elusive (Harris et al., 2006).

YY1 acts on target genes via the recruitment of co-factors, and elucidating YY1 partners may unveil the molecular mechanisms underlying the lung phenotype. For instance, YY1 recruits protein modifiers, such as Ezh2 and histone deacetylases (HDAC), that mediate posttranslational modifications involved in chromatin remodeling (Deng et al., 2010). The epithelial deletion of *Ezh2* function does not cause cyst formation (Snitow et al., 2015). Conversely, the combined epithelial mutations of *Hdac1* and *Hdac2* genes led to airway dilation and to upregulated *Cdkn1a* expression, raising the possibility that YY1 and HDAC act together to some extent during lung morphogenesis (Wang et al., 2013).

Aberrations in lung developmental processes may give rise to structural abnormalities, such as congenital cystic diseases that encompass a spectrum of rare but clinically significant conditions like CCAM and PPB. PPB is characterized in its earliest manifestation by large cysts lined by an alveolar-type epithelium and is often mistaken for CCAM. However, cyst epithelium from CCAM presents a bronchial-like appearance (Hill et al., 2008). There is no known genetic cause for CCAM (Kotecha et al., 2012). Conversely, heterozygous germ line *DICER1* mutations were identified as one major predisposing factor for developing PPB or related conditions such as cystic nephroma and ovarian tumors (Boman et al., 2006; Hill et al., 2009; Slade et al., 2011; Messinger et al., 2015; Pugh et al., 2014). It is proposed that the loss of *DICER1* function occurs primarily in the non-neoplastic epithelial component of the tumor, leading to dysregulation of tumor-promoting factors that stimulate proliferation of the mesenchyme and predispose primitive mesenchymal cells to sarcomatous transformation (Hill et al., 2009). Heterozygous germ line *DICER1* loss-of-function mutations were found in patients with both sporadic and familial PPB. However, carriers with one *DICER1* mutated allele are phenotypically normal, suggesting that secondary genetic events are required for tumor formation. About 30% of PPB patients do not have mutations in the *DICER1* gene further supporting the implication of other genes (Messinger et al., 2015).

A whole exome sequencing analysis of PPB patients revealed somatic *DICER1* missense mutations, but no *YY1* mutations were found (Pugh et al., 2014). The somatic *DICER1* mutations were mainly localized in the RNaseIIIb domain responsible for the cleavage of the 3′end from the -5p strand of microRNA precursors. Mutations of the RNaseIIIb domain were shown to cause a -3p mature microRNA strand bias due to the loss of -5p strand cleavage of the pre-microRNAs (Anglesio et al., 2013).

Development (2015) 142, 2981-2995 doi:10.1242/dev.120469

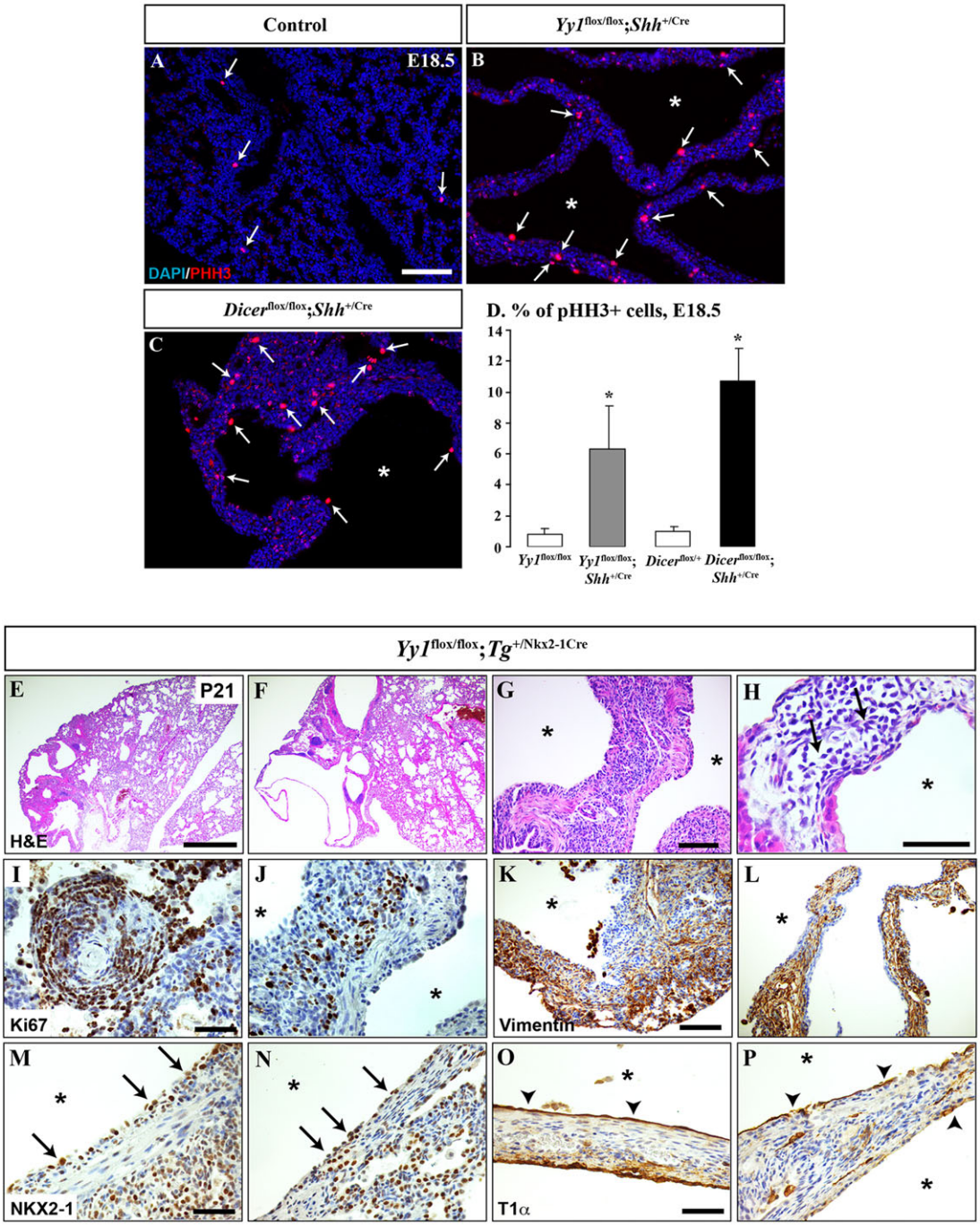

Fig. 9. *Yy1*$^{flox/flox}$;*Tg*$^{Nkx2\text{-}1Cre}$ mice present characteristics of an evolving type I pleuropulmonary blastoma-like phenotype. (A-D) pHH3-positive cells (A-C, arrows) revealed increased proliferation (D) in lungs from E18.5 *Yy1*$^{flox/flox}$;*Shh*$^{+/Cre}$ and *Dicer*$^{flox/flox}$;*Shh*$^{+/Cre}$ embryos. Values are expressed as mean±s.d.; **P*<0.05. (E-H) H&E-stained lung sections from P21 *Yy1*$^{flox/flox}$;*Tg*$^{+/Nkx2\text{-}1Cre}$ mice exhibited alterations in lung architecture with multilocular cysts and variable septal thickness. Arrows in H indicate primitive small mesenchymal cells within the cyst walls. (I,J) Ki67 IHC showed high proliferation levels of mesenchymal cells within the cystic wall. (K-N) Vimentin immunostaining confirmed the mesenchymal identity of the cystic walls (K,L) whereas NKX2-1 IHC established the epithelial nature of the cells lining the cyst (M,N; arrows). (O,P) T1α-positive cells (arrowheads) along the cystic epithelium revealed its alveolar nature. Asterisks indicate cysts. Scale bars: 100 µm in A-C,G,K,L; 1 mm in E,F; 50 µm in H-J,M-P.

Serum microRNA profiling from a PPB patient carrying a somatic mutation in the *DICER1* RNaseIIIb domain showed the overexpression of microRNAs largely derived from the -3p strand (Murray et al., 2014). Among the microRNAs presenting the higher fold change were *let-7a*-3p and *let-7b*-3p, which are predicted to target the human *YY1* gene (http://mirdb.org). It is tempting to speculate that abnormal levels of particular miRNAs may alter YY1 expression providing a mechanistic explanation for the reduced YY1 levels seen in lungs from PPB patients (Fig. 10).

Because *YY1* expression and function are closely associated with cell-cycle progression and apoptosis, the potential role of YY1 in cancer was extensively explored. Both increased and decreased *YY1* expression levels were linked to a wide range of cancers (Wang et al.,

Development (2015) 142, 2981-2995 doi:10.1242/dev.120469

Table 2. Ratios of genotypes in litters from crosses between *Yy1*$^{flox/+}$;*Tg*$^{+/Nkx2\text{-}1Cre}$ and *Yy1*$^{flox/flox}$ mice

Yy1$^{flox/+}$;*Tg*$^{+/Nkx2\text{-}1Cre}$×*Yy1*$^{flox/flox}$

					Tg$^{+/Nkx2\text{-}1Cre}$	
Age	# litters	# pups	*Yy1*$^{flox/+}$	*Yy1*$^{flox/flox}$	*Yy1*$^{flox/+}$	*Yy1*$^{flox/flox}$
Expected (%)			(25)	(25)	(25)	(25)
E14.5	3	23	9 (39.1)	7 (30.4)	2 (8.8)	5 (21.7)
E18.5	2	14	4 (28.6)	4 (28.6)	3 (21.4)	3 (21.4)
P21	14	86	17 (19.8)	37 (43)	25 (29.1)	7 (8.1)

The percentage obtained is indicated in parentheses.

2008; Nicholson et al., 2011). Analysis of *Yy1*$^{flox/flox}$;*Shh*$^{+/Cre}$ lungs at late gestation revealed a burst in cell proliferation in both epithelium and mesenchyme that may reflect a potential subsequent malignant transformation. The reduced expressivity of the lung phenotype of *Yy1*$^{flox/flox}$;*Tg*$^{+/Nkx2\text{-}1Cre}$ mutants allowed us to overcome the neonatal death of *Yy1*$^{flox/flox}$;*Shh*$^{+/Cre}$ pups. The cystic architectural and histological features observed in mutant mice were reminiscent of an evolving type I PPB, further supporting the notion that reduced expression of YY1 may participate in PPB pathogenesis. It must be underscored that the unrepressed *Fgf10* expression seen in *Yy1* mutants should also be considered to play a role in cancer development as *Fgf10* overexpression in the lung during the postnatal period can cause multifocal pulmonary tumors (Clark et al., 2001).

In conclusion, we present evidence of the crucial role played by the transcription factor YY1 in the developing epithelium of the respiratory tract for lung branching morphogenesis. Although further works are needed to fully elucidate the underlying mechanisms, SHH appears to be a key player in mediating YY1 function in the lung. Our *Yy1* mouse models also reproduced characteristics of the rare early childhood cancer PPB and indicated that a more precise gene dosage mouse model operating within the context of a developmental window should provide a strong model for the exploration of PPB molecular pathogenesis.

MATERIALS AND METHODS

Mice, genotyping and tissue collection

Yy1$^{flox/flox}$ mice were obtained from Dr Shi (Affar et al., 2006). The *Rosa26* reporter line [*Gt(ROSA)26Sor*$^{tm4(ACTB\text{-}tdTomato,\text{-}EGFP)Luo}$], the *Dicer1*$^{flox/flox}$ conditional line (*Dicer1*$^{tm1Bdh/J}$), and the *Shh*^{Cre} [*Shh*$^{tm1(EGFP/cre)Cjt}$] and *Tg*$^{+/Nkx2\text{-}1Cre}$ [Tg$^{(Nkx2\text{-}1\text{-}cre)2Sand}$] deleter strains were purchased from The Jackson Laboratory (Harfe et al., 2004, 2005; Muzumdar et al., 2007; Xu et al., 2008). As only individuals carrying the *Yy1*$^{flox/flox}$;*Shh*$^{+/Cre}$, *Yy1*$^{flox/flox}$;*Nkx2-1-Cre* and *Dicer*$^{flox/flox}$;*Shh*$^{+/Cre}$ genotypes presented defects, all the other genotypes were referred hereafter as controls except when specified. Age of the embryos was estimated by considering the morning of the day of the vaginal plug as E0.5. Experimental specimens were genotyped by PCR analyses. Lungs were collected at E12.5, E14.5, E18.5 or postnatal day (P) 21 as described (Boucherat et al., 2014). For RNA extraction, lungs were snap-frozen in N_2. Experiments were performed according to the guidelines of the Canadian Council on Animal Care and approved by the institutional animal care committee.

Human tissues

This study was conducted with anonymised specimens of CCAM and PPB patients from the Department of Pathology of Hôpital Necker-Enfants Malades, Paris, France and from McGill University, Montréal, Canada and

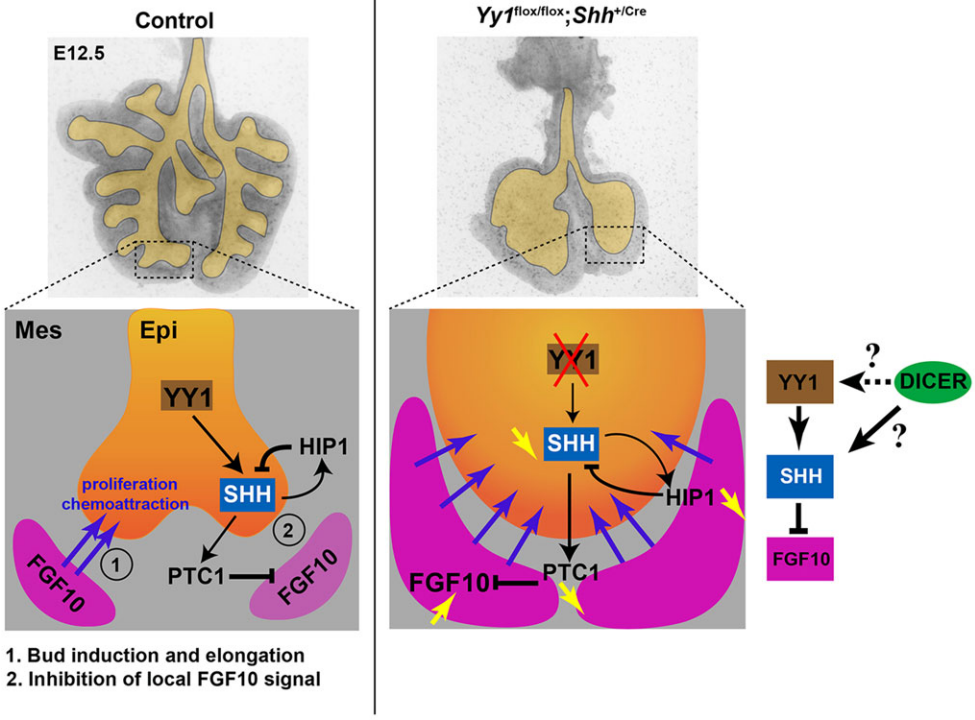

Fig. 10. Model for the action of YY1 during lung branching morphogenesis. During lung branching morphogenesis, FGF10 localization and expression are dynamically regulated within the mesenchyme to induce epithelial proliferation and budding. Once the epithelial buds start to elongate, activation of the SHH signaling pathway occurs as a negative feedback mechanism. Consequently, the subepithelial mesenchyme proliferates, FGF10 expression levels near the bud tips decrease and FGF10-expressing foci shift laterally, promoting a next round of branching. In the absence of *Yy1* function in lung epithelium, *Shh* expression is reduced, causing an increased and diffuse expression of FGF10 throughout the mesenchyme. Lung branching is impaired, resulting in rudimentary lungs with large epithelial cysts. The unrestricted and elevated FGF10 expression represents a reasonable primary cause of airway dilation in the developing lung. Similar changes are observed in *Dicer*$^{flox/flox}$;*Shh*$^{+/Cre}$ mice. However, the mechanisms of DICER action in lung epithelium are still unknown.

Development (2015) 142, 2981-2995 doi:10.1242/dev.120469

approved by the respective Ethics Committee. Controls corresponded to normal lung specimens from the Department of Pathology of Hôpital Raymond Poincaré, Garches, France. They were collected at autopsy from age-matched children who died from a non-pulmonary cause (sudden infant death syndrome). Characteristics of patients are summarized in supplementary material Table S1.

Histology, immunohistochemistry (IHC) and immunofluorescence (IF) analyses

Experiments were performed as described (Boucherat et al., 2014). The Cyanine 3 Tyramide Signal Amplification Kit (PerkinElmer) was used for pERK detection. Antibodies are listed in supplementary material Table S2.

Proliferation and apoptosis

Experiments were performed as described (Boucherat et al., 2014). Three to four random fields were taken, for an average number of 650 cells per field, from four to five embryos per genotype.

In situ hybridization

RNA *in situ* hybridization was performed on 15 µm cryosections of E12.5 embryos (Schaeren-Wiemers and Gerfin-Moser, 1993). A 584-bp mouse *Fgf10* cDNA fragment was used for the digoxigenin-labeled riboprobe (provided by Dr B. Hogan, Duke University Medical Center, USA). Experiments were performed on four specimens per genotype.

Alcian Blue cartilage staining

Dissected respiratory tracts from E18.5 embryos were stained in a solution of 0.03% Alcian Blue and 20% acetic acid prepared in 95% ethanol. The external tracheal diameter was measured at five rostrocaudal locations along the most linear portion of the trachea and quantified using NIH ImageJ software. Tracheal luminal surface was measured using Leica SCN 400 F SlideScanner and SlidePath Gateway Software.

Quantitative RT-PCR (qRT-PCR)

Lung total RNA was isolated from individual E14.5 embryos. qRT-PCR experiments were performed as described (Boucherat et al., 2012). Three to eight specimens were used per genotype tested. Primer sequences are listed in supplementary material Table S3A.

Chromatin immunoprecipitation (ChIP) assays

Lungs from E14.5 wild-type embryos were collected and ChIP assay was performed with rabbit anti-YY1 antibody, rabbit anti-histone H3, or control rabbit IgG as described (Bérubé-Simard et al., 2014). qPCR-ChIP analyses were performed with primers specific to each domain containing YY1 binding sites (supplementary material Table S3B). The values for the samples immunoprecipitated by anti-YY1, anti-histone H3, or control IgG were recorded as the percentage relative to input. ChIP results were confirmed by two independent experiments. qPCR was performed in triplicate for each sample. ChIP efficiency was calculated by dividing the amount of PCR product obtained with the immunoprecipitated DNA by the amount obtained with the input DNA (Aparicio et al., 2005).

Transactivation assays

Human pCMV-YY1 and control pCMV-GFP-LpA expression vectors were obtained from Drs G. Blanck (University of South Florida, USA) and R. Aasland (University of Bergen, Norway), respectively. A 5-kb *Bgl*II-*Xho*I genomic fragment located between positions −5016 bp and +60 bp of the mouse *Shh* gene (relative to TSS) was cloned into the pGL3 basic luciferase reporter expression plasmid (Promega). HEK293 cells were transiently co-transfected in 24-well plates (40,000 cells/well) with 0.3 µg/well of luciferase reporter construct and 0.2 µg/well of YY1 or control expression vectors using the FuGENE 6 transfection reagent (Promega). The RL-SV40 *Renilla reniformis* luciferase expression vector (Promega) was used as an internal control for transfection efficiency (0.001 µg/well). Luciferase activity was measured 48 h after transfection with the Dual-Luciferase Reporter Assay System (Promega). Transfections were performed in triplicate in at least two independent experiments. Data from a representative experiment are presented as the fold induction±s.d. of normalized relative luciferase activity.

Lung explant cultures

Experiments were performed as described (Boucherat et al., 2014). Lungs were kept for 72 h in serum-free DMEM/F12 medium (Gibco) in presence or not of rmSHH protein, N-Terminus (R&D Systems) at a concentration of 3 µg/ml. BSA was used as control.

Microarray analysis

Total RNA was isolated from lungs of E14.5 $Shh^{+/Cre}$, $Yy1^{flox/flox}$;$Shh^{+/Cre}$ and $Dicer^{flox/flox}$;$Shh^{+/Cre}$ embryos (n=4/genotype). RNA quality and quantity assessment, cDNA probe preparation, hybridization to the Affymetrix Mouse Gene 2.0ST Array and image scan were performed at the Genome Quebec Innovation Centre at McGill University (Montréal, Canada). Data were pre-processed and normalized using Affymetrix Power Tools with the rma-sketch method. Raw and normalized data were uploaded to the NCBI Gene Expression Omnibus database (http://www.ncbi.nlm.nih.gov/projects/geo) with the accession number GSE66171 according to MIAME standards (Edgar et al., 2002). Significantly modulated probes were identified using the empirical Bayes statistics available in limma (Smyth, 2004). Probes were considered to be significantly modulated when the Benjamini–Hochberg-adjusted was significant to P<0.05.

Statistical analyses

Student's t-test was performed for comparative studies. A significance level inferior to 5% (P<0.05) was considered statistically significant.

Acknowledgements

We thank Drs Y. Shi for *Yy1* mice, R. Aasland, G. Blanck, B. Hogan and G. Singh for sharing reagents, P. Joubert and B. Têtu for advice in histopathology, M. Simard for judicious comments, V. Nadeau for technical help and E. Paquet for microarray data analysis.

Competing interests

The authors declare no competing or financial interests.

Author contributions

O.B. and L.J. designed the experiments; O.B., K.L.-T, F.-A.B.-S., N.H., L.B. performed the experiments; G.L., W.D.F. and C.D. provide human specimens, O.B., K.L.-T, F.-A.B.-S., N.H., L.B., J.C. and L.J. analyzed the data; O.B. and L.J. wrote the paper.

Funding

This work was supported by grants from the Canadian Institutes of Health Research [MOP-15139, L.J.; MOP-97801, J.C.], Natural Sciences and Engineering Research Council of Canada [194559, L.J.], The Cancer Research Society (L.J.) and Université Laval Foundation (L.J.).

Supplementary material

Supplementary material available online at
http://dev.biologists.org/lookup/suppl/doi:10.1242/dev.120469/-/DC1

References

Affar, E. B., Gay, F., Shi, Y., Liu, H., Huarte, M., Wu, S., Collins, T., Li, E. and Shi, Y. (2006). Essential dosage-dependent functions of the transcription factor yin yang 1 in late embryonic development and cell cycle progression. *Mol. Cell. Biol.* **26**, 3565-3581.

Anglesio, M. S., Wang, Y., Yang, W., Senz, J., Wan, A., Heravi-Moussavi, A., Salamanca, C., Maines-Bandiera, S., Huntsman, D. G. and Morin, G. B. (2013). Cancer-associated somatic DICER1 hotspot mutations cause defective miRNA processing and reverse-strand expression bias to predominantly mature 3p strands through loss of 5p strand cleavage. *J. Pathol.* **229**, 400-409.

Aparicio, O., Geisberg, J. V., Sekinger, E., Yang, A., Moqtaderi, Z. and Struhl, K. (2005). Chromatin immunoprecipitation for determining the association of proteins with specific genomic sequences *in vivo*. *Curr. Protoc. Mol. Biol.* **21.3**,1-33.

Aubin, J., Lemieux, M., Tremblay, M., Bérard, J. and Jeannotte, L. (1997). Early postnatal lethality in Hoxa-5 mutant mice is attributable to respiratory tract defects. *Dev. Biol.* **192**, 432-445.

Bartel, D. P. (2004). MicroRNAs: genomics, biogenesis, mechanism, and function. *Cell* **116**, 281-297.

Bellusci, S., Grindley, J., Emoto, H., Itoh, N. and Hogan, B. L. (1997). Fibroblast growth factor 10 (FGF10) and branching morphogenesis in the embryonic mouse lung. *Development* **124**, 4867-4878.

Bérubé-Simard, F.-A., Prudhomme, C. and Jeannotte, L. (2014). YY1 acts as a transcriptional activator of *Hoxa5* gene expression in mouse organogenesis. *PLoS ONE* **9**, e93989.

Boman, F., Hill, D. A., Williams, G. M., Chauvenet, A., Fournet, J.-C., Soglio, D. B.-D., Messinger, Y. and Priest, J. R. (2006). Familial association of pleuropulmonary blastoma with cystic nephroma and other renal tumors: a report from the International Pleuropulmonary Blastoma Registry. *J. Pediatr.* **149**, 850-854.e2.

Boucherat, O., Chakir, J. and Jeannotte, L. (2012). The loss of *Hoxa5* function promotes Notch-dependent goblet cell metaplasia in lung airways. *Biol. Open* **1**, 677-691.

Boucherat, O., Nadeau, V., Bérubé-Simard, F.-A., Charron, J. and Jeannotte, L. (2014). Crucial requirement of ERK/MAPK signaling in respiratory tract development. *Development* **141**, 3197-3211.

Chang, D. R., Martinez Alanis, D., Miller, R. K., Ji, H., Akiyama, H., McCrea, P. D. and Chen, J. (2013). Lung epithelial branching program antagonizes alveolar differentiation. *Proc. Natl. Acad. Sci. USA* **110**, 18042-18051.

Chuang, P.-T. and McMahon, A. P. (1999). Vertebrate Hedgehog signalling modulated by induction of a Hedgehog-binding protein. *Nature* **397**, 617-621.

Clark, J. C., Tichelaar, J. W., Wert, S. E., Itoh, N., Perl, A. K., Stahlman, M. T. and Whitsett, J. A. (2001). FGF-10 disrupts lung morphogenesis and causes pulmonary adenomas in vivo. *Am. J. Physiol. Lung Cell Mol. Physiol.* **280**, L705-L715.

del Moral, P.-M., De Langhe, S. P., Sala, F. G., Veltmaat, J. M., Tefft, D., Wang, K., Warburton, D. and Bellusci, S. (2006). Differential role of FGF9 on epithelium and mesenchyme in mouse embryonic lung. *Dev. Biol.* **293**, 77-89.

Deng, Z., Cao, P., Wan, M. M. and Sui, G. (2010). Yin Yang 1: a multifaceted protein beyong a transcription factor. *Transcription* **1**, 81-84.

Donohoe, M. E., Zhang, X., McGinnis, L., Biggers, J., Li, E. and Shi, Y. (1999). Targeted disruption of mouse Yin Yang 1 transcription factor results in peri-implantation lethality. *Mol. Cell. Biol.* **19**, 7237-7244.

Donohoe, M. E., Zhang, L.-F., Xu, N., Shi, Y. and Lee, J. T. (2007). Identification of a Ctcf cofactor, Yy1, for the X chromosome binary switch. *Mol. Cell* **25**, 43-56.

Edgar, R., Domrachev, M. and Lash, A. E. (2002). Gene Expression Omnibus: NCBI gene expression and hybridization array data repository. *Nucleic Acids Res.* **30**, 207-210.

Gonzaga, S., Henriques-Coelho, T., Davey, M., Zoltick, P. W., Leite-Moreira, A. F., Correia-Pinto, J. and Flake, A. W. (2008). Cystic adenomatoid malformations are induced by localized FGF10 overexpression in fetal rat lung. *Am. J. Respir. Cell Mol. Biol.* **39**, 346-355.

Gordon, S., Akopyan, G., Garban, H. and Bonavida, B. (2006). Transcription factor YY1: structure, function, and therapeutic implications in cancer biology. *Oncogene* **25**, 1125-1142.

Harfe, B. D., Scherz, P. J., Nissim, S., Tian, H., McMahon, A. P. and Tabin, C. J. (2004). Evidence for an expansion-based temporal Shh gradient in specifying vertebrate digit identities. *Cell* **118**, 517-528.

Harfe, B. D., McManus, M. T., Mansfield, J. H., Hornstein, E. and Tabin, C. J. (2005). The RNaseIII enzyme Dicer is required for morphogenesis but not patterning of the vertebrate limb. *Proc. Natl. Acad. Sci. USA* **102**, 10898-10903.

Harris, K. S., Zhang, Z., McManus, M. T., Harfe, B. D. and Sun, X. (2006). Dicer function is essential for lung epithelium morphogenesis. *Proc. Natl. Acad. Sci. USA* **103**, 2208-2213.

Hill, D. A., Jarzembowski, J. A., Priest, J. R., Williams, G., Schoettler, P. and Dehner, L. P. (2008). Type I pleuropulmonary blastoma: pathology and biology study of 51 cases from the international pleuropulmonary blastoma registry. *Am. J. Surg. Pathol.* **32**, 282-295.

Hill, D. A., Ivanovich, J., Priest, J. R., Gurnett, C. A., Dehner, L. P., Desruisseau, D., Jarzembowski, J. A., Wikenheiser-Brokamp, K. A., Suarez, B. K., Whelan, A. J. et al. (2009). DICER1 mutations in familial pleuropulmonary blastoma. *Science* **325**, 965.

Kang, K., Chung, J. H. and Kim, J. (2009). Evolutionary Conserved Motif Finder (ECMFinder) for genome-wide identification of clustered YY1- and CTCF-binding sites. *Nucleic Acids Res.* **37**, 2003-2013.

Kimura, S., Hara, Y., Pineau, T., Fernandez-Salguero, P., Fox, C. H., Ward, J. M. and Gonzalez, F. J. (1996). The T/ebp null mouse: thyroid-specific enhancer-binding protein is essential for the organogenesis of the thyroid, lung, ventral forebrain, and pituitary. *Genes Dev.* **10**, 60-69.

Kotecha, S., Barbato, A., Bush, A., Claus, F., Davenport, M., Delacourt, C., Deprest, J., Eber, E., Frenckner, B., Greenough, A. et al. (2012). Antenatal and postnatal management of congenital cystic adenomatoid malformation. *Paediatr. Respir. Rev.* **13**, 162-171.

Litingtung, Y., Lei, L., Westphal, H. and Chiang, C. (1998). Sonic hedgehog is essential to foregut development. *Nat. Genet.* **20**, 58-61.

Liu, Y., Jiang, H., Crawford, H. C. and Hogan, B. L. M. (2003). Role for ETS domain transcription factors Pea3/Erm in mouse lung development. *Dev. Biol.* **261**, 10-24.

Mahlapuu, M., Enerbäck, S. and Carlsson, P. (2001). Haploinsufficiency of the forkhead gene Foxf1, a target for sonic hedgehog signaling, causes lung and foregut malformations. *Development* **128**, 2397-2406.

Mailleux, A. A., Tefft, D., Ndiaye, D., Itoh, N., Thiery, J. P., Warburton, D. and Bellusci, S. (2001). Evidence that SPROUTY2 functions as an inhibitor of mouse embryonic lung growth and morphogenesis. *Mech. Dev.* **102**, 81-94.

Messinger, Y. H., Stewart, D. R., Priest, J. R., Williams, G. M., Harris, A. K., Schultz, K. A. P., Yang, J., Doros, L., Rosenberg, P. S., Hill, D. A. et al. (2015). Pleuropulmonary blastoma: a report on 350 central pathology-confirmed pleuropulmonary blastoma cases by the International Pleuropulmonary Blastoma Registry. *Cancer* **121**, 276-285.

Metzger, D. E., Xu, Y. and Shannon, J. M. (2007). Elf5 is an epithelium-specific, fibroblast growth factor-sensitive transcription factor in the embryonic lung. *Dev. Dyn.* **236**, 1175-1192.

Metzger, D. E., Stahlman, M. T. and Shannon, J. M. (2008). Misexpression of ELF5 disrupts lung branching and inhibits epithelial differentiation. *Dev. Biol.* **320**, 149-160.

Minoo, P., Su, G., Drum, H., Bringas, P. and Kimura, S. (1999). Defects in tracheoesophageal and lung morphogenesis in Nkx2.1(−/−) mouse embryos. *Dev. Biol.* **209**, 60-71.

Morrisey, E. E. and Hogan, B. L. M. (2010). Preparing for the first breath: genetic and cellular mechanisms in lung development. *Dev. Cell* **18**, 8-23.

Murray, M. J., Bailey, S., Raby, K. L., Saini, H. K., de Kock, L., Burke, G. A. A., Foulkes, W. D., Enright, A. J., Coleman, N. and Tischkowitz, M. (2014). Serum levels of mature microRNAs in DICER1-mutated pleuropulmonary blastoma. *Oncogenesis* **3**, e87.

Muzumdar, M. D., Tasic, B., Miyamichi, K., Li, L. and Luo, L. (2007). A global double-fluorescent Cre reporter mouse. *Genesis* **45**, 593-605.

Nicholson, S., Whitehouse, H., Naidoo, K. and Byers, R. (2011). Yin Yang 1 in human cancer. *Crit. Rev. Oncog.* **16**, 245-260.

Park, J., Zhang, J. J. R., Moro, A., Kushida, M., Wegner, M. and Kim, P. C. W. (2010). Regulation of Sox9 by Sonic Hedgehog (Shh) is essential for patterning and formation of tracheal cartilage. *Dev. Dyn.* **239**, 514-526.

Pepicelli, C. V., Lewis, P. M. and McMahon, A. P. (1998). Sonic hedgehog regulates branching morphogenesis in the mammalian lung. *Curr. Biol.* **8**, 1083-1086.

Pugh, T. J., Yu, W., Yang, J., Field, A. L., Ambrogio, L., Carter, S. L., Cibulskis, K., Giannikopoulos, P., Kiezun, A., Kim, J. et al. (2014). Exome sequencing of pleuropulmonary blastoma reveals frequent biallelic loss of TP53 and two hits in DICER1 resulting in retention of 5p-derived miRNA hairpin loop sequences. *Oncogene* **33**, 5295-5302.

Que, J., Luo, X., Schwartz, R. J. and Hogan, B. L. M. (2009). Multiple roles for Sox2 in the developing and adult mouse trachea. *Development* **136**, 1899-1907.

Rock, J. R., Onaitis, M. W., Rawlins, E. L., Lu, Y., Clark, C. P., Xue, Y., Randell, S. H. and Hogan, B. L. M. (2009). Basal cells as stem cells of the mouse trachea and human airway epithelium. *Proc. Natl. Acad. Sci. USA* **106**, 12771-12775.

Schaeren-Wiemers, N. and Gerfin-Moser, A. (1993). A single protocol to detect transcripts of various types and expression levels in neural tissue and cultured cells: in situ hybridization using digoxigenin-labelled cRNA probes. *Histochemistry* **100**, 431-440.

Shu, W., Lu, M. M., Zhang, Y., Tucker, P. W., Zhou, D. and Morrisey, E. E. (2007). Foxp2 and Foxp1 cooperatively regulate lung and esophagus development. *Development* **134**, 1991-2000.

Slade, I., Bacchelli, C., Davies, H., Murray, A., Abbaszadeh, F., Hanks, S., Barfoot, R., Burke, A., Chisholm, J., Hewitt, M. et al. (2011). DICER1 syndrome: clarifying the diagnosis, clinical features and management implications of a pleiotropic tumour predisposition syndrome. *J. Med. Genet.* **48**, 273-278.

Smyth, G. K. (2004). Linear models and empirical bayes methods for assessing differential expression in microarray experiments. *Stat. Appl. Genet. Mol. Biol.* **3**, 1-25.

Snitow, M. E., Li, S., Morley, M. P., Rathi, K., Lu, M. M., Kadzik, R. S., Stewart, K. M. and Morrisey, E. E. (2015). Ezh2 represses the basal cell lineage during lung endoderm development. *Development* **142**, 108-117.

Stocker, J. T. (2009). Cystic lung disease in infants and children. *Fetal Pediatr. Pathol.* **28**, 155-184.

Tian, Y., Zhang, Y., Hurd, L., Hannenhalli, S., Liu, F., Lu, M. M. and Morrisey, E. E. (2011). Regulation of lung endoderm progenitor cell behavior by miR302/367. *Development* **138**, 1235-1245.

Tsukui, T., Capdevila, J., Tamura, K., Ruiz-Lozano, P., Rodriguez-Esteban, C., Yonei-Tamura, S., Magallón, J., Chandraratna, R. A. S., Chien, K., Blumberg, B. et al. (1999). Multiple left-right asymmetry defects in Shh(−/−) mutant mice unveil a convergence of the shh and retinoic acid pathways in the control of Lefty-1. *Proc. Natl. Acad. Sci. USA* **96**, 11376-11381.

van Tuyl, M., Liu, J., Groenman, F., Ridsdale, R., Han, R. N. N., Venkatesh, V., Tibboel, D. and Post, M. (2006). Iroquois genes influence proximo-distal morphogenesis during rat lung development. *Am. J. Physiol. Lung Cell Mol. Physiol.* **290**, L777-L789.

van Tuyl, M., Groenman, F., Wang, J., Kuliszewski, M., Liu, J., Tibboel, D. and Post, M. (2007). Angiogenic factors stimulate tubular branching morphogenesis of sonic hedgehog-deficient lungs. *Dev. Biol.* **303**, 514-526.

Volckaert, T., Campbell, A., Dill, E., Li, C., Minoo, P. and De Langhe, S. (2013). Localized Fgf10 expression is not required for lung branching morphogenesis but prevents differentiation of epithelial progenitors. *Development* **140**, 3731-3742.
Wan, H., Xu, Y., Ikegami, M., Stahlman, M. T., Kaestner, K. H., Ang, S.-L. and Whitsett, J. A. (2004). Foxa2 is required for transition to air breathing at birth. *Proc. Natl. Acad. Sci. USA* **101**, 14449-14454.
Wang, H., Garzon, R., Sun, H., Ladner, K. J., Singh, R., Dahlman, J., Cheng, A., Hall, B. M., Qualman, S. J., Chandler, D. S. et al. (2008). NF-kappaB-YY1-miR-29 regulatory circuitry in skeletal myogenesis and rhabdomyosarcoma. *Cancer Cell* **14**, 369-381.
Wang, X., Wolgemuth, D. J. and Baxi, L. V. (2011). Overexpression of HOXB5, cyclin D1 and PCNA in congenital cystic adenomatoid malformation. *Fetal Diagn. Ther.* **29**, 315-320.
Wang, Y., Tian, Y., Morley, M. P., Lu, M. M., Demayo, F. J., Olson, E. N. and Morrisey, E. E. (2013). Development and regeneration of Sox2+ endoderm progenitors are regulated by a Hdac1/2-Bmp4/Rb1 regulatory pathway. *Dev. Cell* **24**, 345-358.
Weaver, M., Dunn, N. R. and Hogan, B. L. (2000). Bmp4 and Fgf10 play opposing roles during lung bud morphogenesis. *Development* **127**, 2695-2704.
White, A. C., Xu, J., Yin, Y., Smith, C., Schmid, G. and Ornitz, D. M. (2006). FGF9 and SHH signaling coordinate lung growth and development through regulation of distinct mesenchymal domains. *Development* **133**, 1507-1517.
Xu, Q., Tam, M. and Anderson, S. A. (2008). Fate mapping Nkx2.1-lineage cells in the mouse telencephalon. *J. Comp. Neurol.* **506**, 16-29.
Yang, J. and Chen, J. (2014). Developmental programs of lung epithelial progenitors: a balanced progenitor model. *Wiley Interdiscip. Rev. Dev. Biol.* **3**, 331-347.
Yin, Y., Wang, F. and Ornitz, D. M. (2011). Mesothelial- and epithelial-derived FGF9 have distinct functions in the regulation of lung development. *Development* **138**, 3169-3177.
Yin, Y., Castro, A. M., Hoekstra, M., Yan, T. J., Kanakamedala, A. C., Dehner, L. P., Hill, D. A. and Ornitz, D. M. (2015). Fibroblast growth factor 9 regulation by microRNAs controls lung development and links *DICER1* loss to the pathogenesis of pleuropulmonary blastoma. *PLoS Genet.* **11**, e1005242.

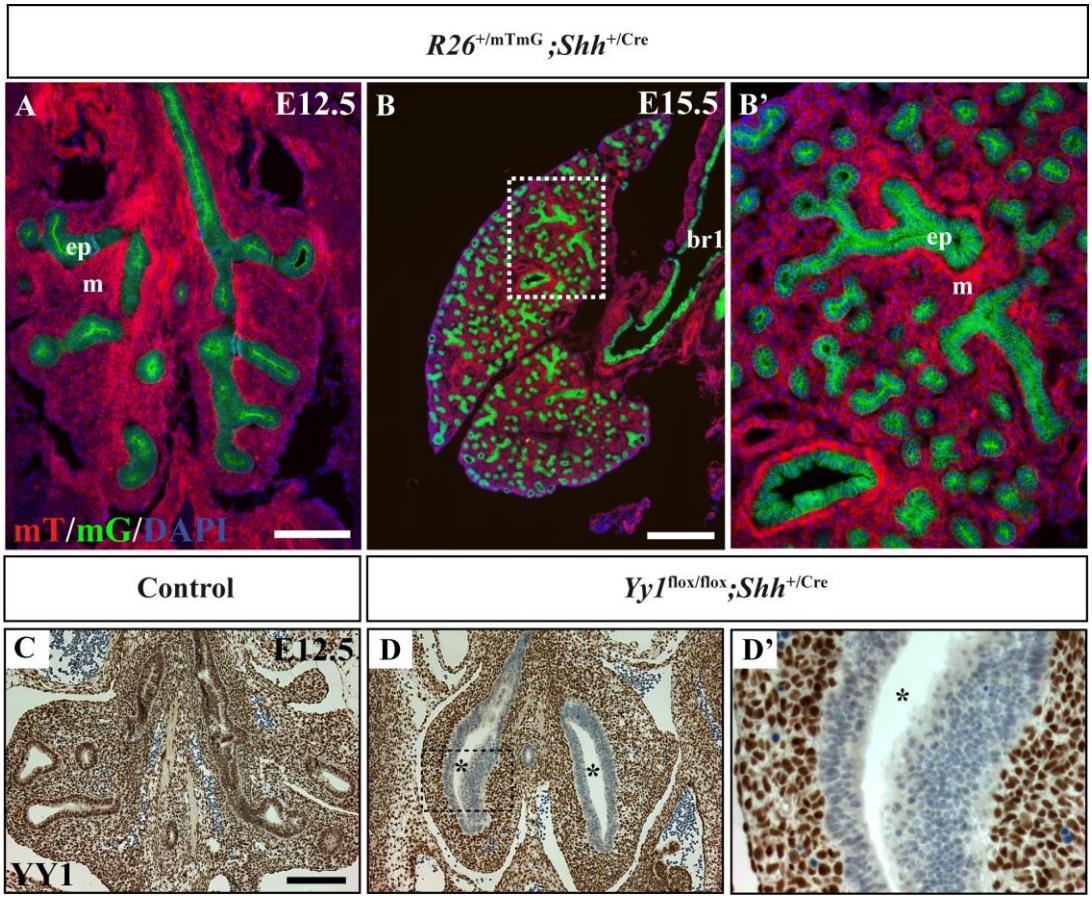

Figure S1. Cre recombinase specificity and efficiency of the *Yy1* deletion by the *Shh*^{Cre} allele in the developing lung. (A,B) Validation of Cre efficiency was assessed by breeding *Shh*$^{+/Cre}$ mice with *R26*$^{mTmG/mTmG}$ reporter mice expressing the membrane-targeted tandem dimer Tomato (mT) prior Cre-mediated excision and membrane-targeted green fluorescent protein (mG) after excision. At E12.5 (A) and E15.5 (B), GFP expression was detected in the respiratory epithelium. No Cre activity was detected in lung mesenchyme. (C,D) YY1 IHC experiments demonstrated the loss of YY1 expression in the respiratory epithelium of E12.5 *Yy1*$^{flox/flox}$;*Shh*$^{+/Cre}$ embryos. Boxed areas in B and D are magnified in B' and D', respectively. Br1, primary bronchi; ep, epithelium; m, mesenchyme. Asterisks indicate cysts. Scale bars: 200 μm (A,C,D), 300 μm (B).

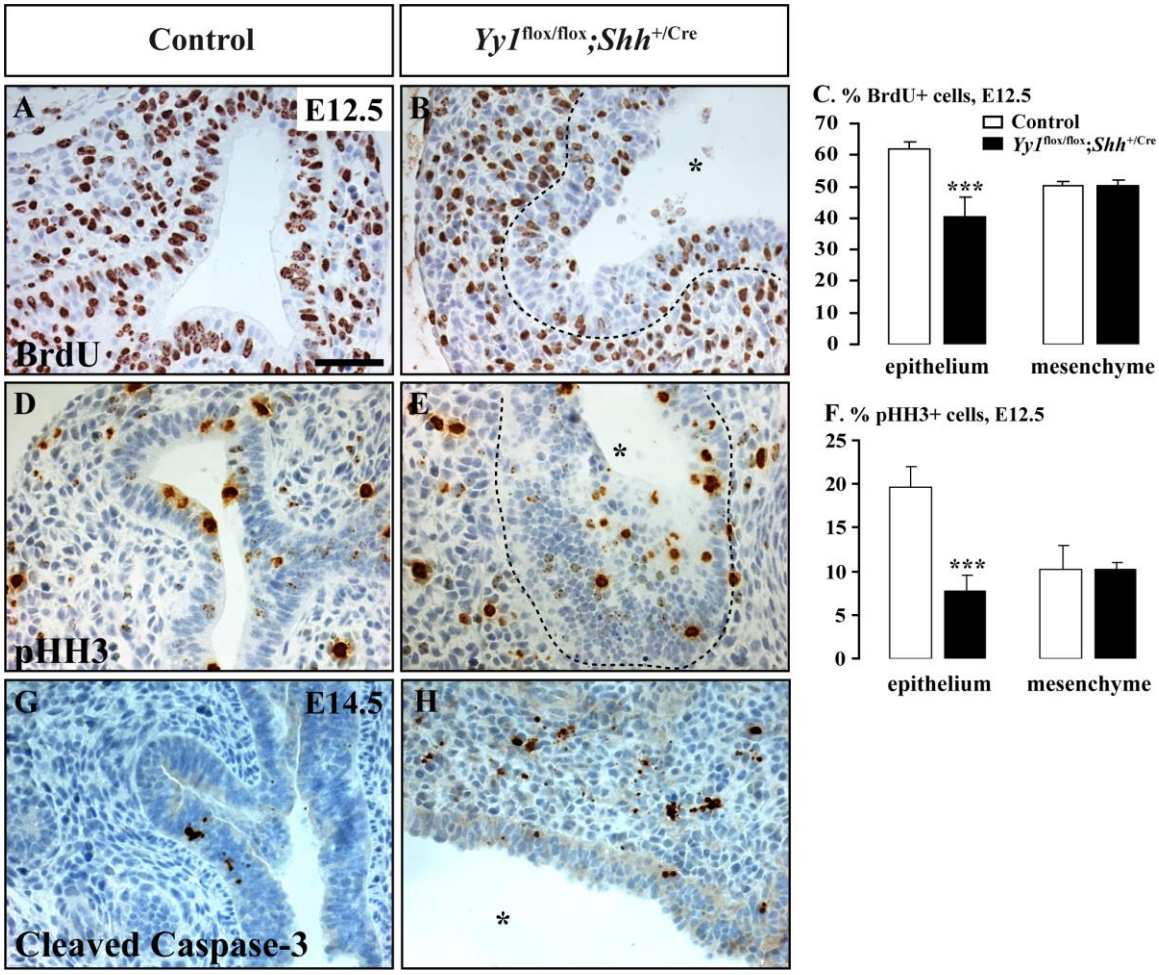

Figure S2. Reduced epithelial proliferation and increased apoptosis in lungs from *Yy1*$^{flox/flox}$;*Shh*$^{+/Cre}$ mutants. (A-C) The number of cells in S-phase, as determined by BrdU pulse-labeling assay, was significantly decreased in lung epithelium from *Yy1*$^{flox/flox}$;*Shh*$^{+/Cre}$ mutants while no change was seen in the mesenchyme. (D-F) Reduced proliferation of lung epithelial cells was also demonstrated by pHH3 immunostaining, a marker for cells in late G2 and mitosis. Thus, *Yy1* is essential for the control of lung epithelial cell proliferation throughout the cell cycle. (G,H) Cleaved caspase-3 immunostaining revealed increased apoptosis in lung mesenchyme of E14.5 *Yy1*$^{flox/flox}$;*Shh*$^{+/Cre}$ specimens. Asterisks indicate cysts. **P<0.01. Scale bar: 50 μm.

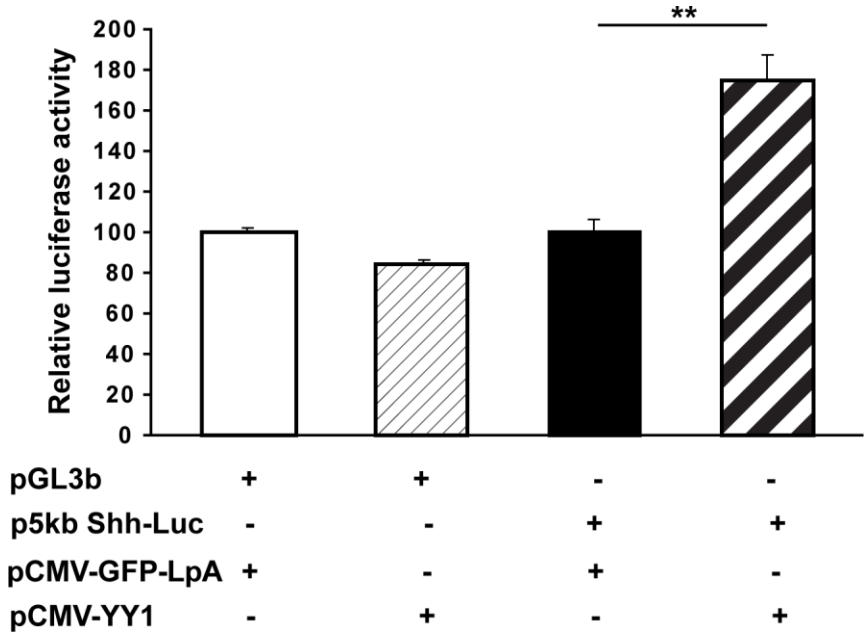

Figure S3. YY1 can activate *Shh* expression in transactivation assays. In a transient transfection assay in HEK293 cells, human YY1 protein upregulated transcription of a luciferase reporter construct containing a 5-kb genomic fragment encompassing *Shh* promoter and upstream sequences. Data from a representative experiment are presented as the fold induction±s.d. of normalized relative luciferase activity. ***P*<0.01

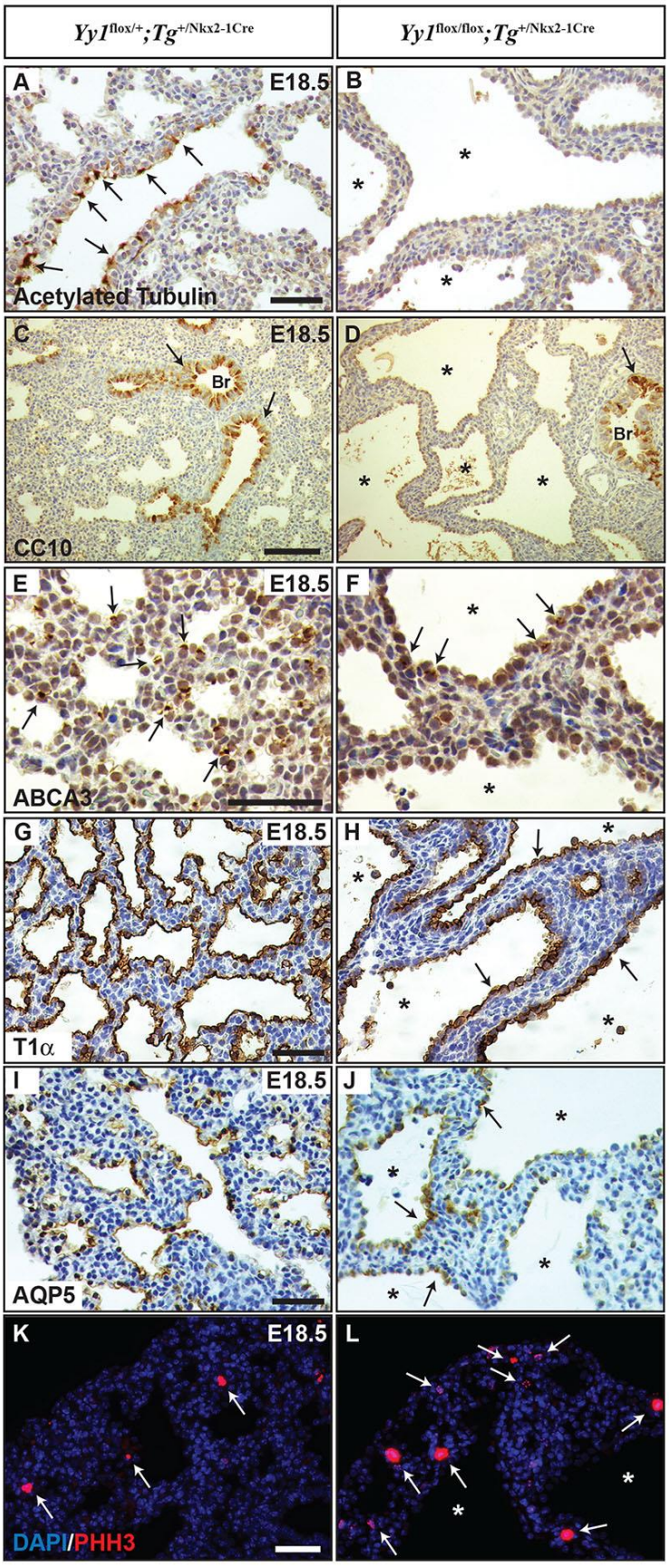
Yy1flox/+;Tg+/Nkx2-1Cre
Yy1flox/flox;Tg+/Nkx2-1Cre
A
E18.5
Acetylated Tubulin
B
C
E18.5
Br
CC10
D
Br
E
E18.5
ABCA3
F
G
E18.5
T1α
H
I
E18.5
AQP5
J
K
E18.5
DAPI/PHH3
L

Figure S4. Abnormal epithelial differentiation and increased cell proliferation in lungs from E18.5 *Yy1*$^{flox/flox}$;*Tg*$^{+/Nkx2\text{-}1Cre}$ embryos. (A-D) Neither ciliated nor club cells, as detected by IHC with acetylated tubulin and CC10 specific markers, respectively, were observed in cyst epithelium of E18.5 *Yy1*$^{flox/flox}$;*Tg*$^{+/Nkx2\text{-}1Cre}$ mutants. (E-J) Cysts were lined by Type II and Type I pneumocytes as revealed by ABCA3 and T1α/AQP5 specific markers, respectively (arrows). (K,L) pHH3-positive cells (arrows) revealed increased proliferation in lungs from E18.5 *Yy1*$^{flox/flox}$; *Tg*$^{+/ Nkx2\text{-}1Cre}$. Br, bronchi. Asterisks indicate cysts. Scale bars: 50 μm (A,B,E-L), 100 μm (C,D).

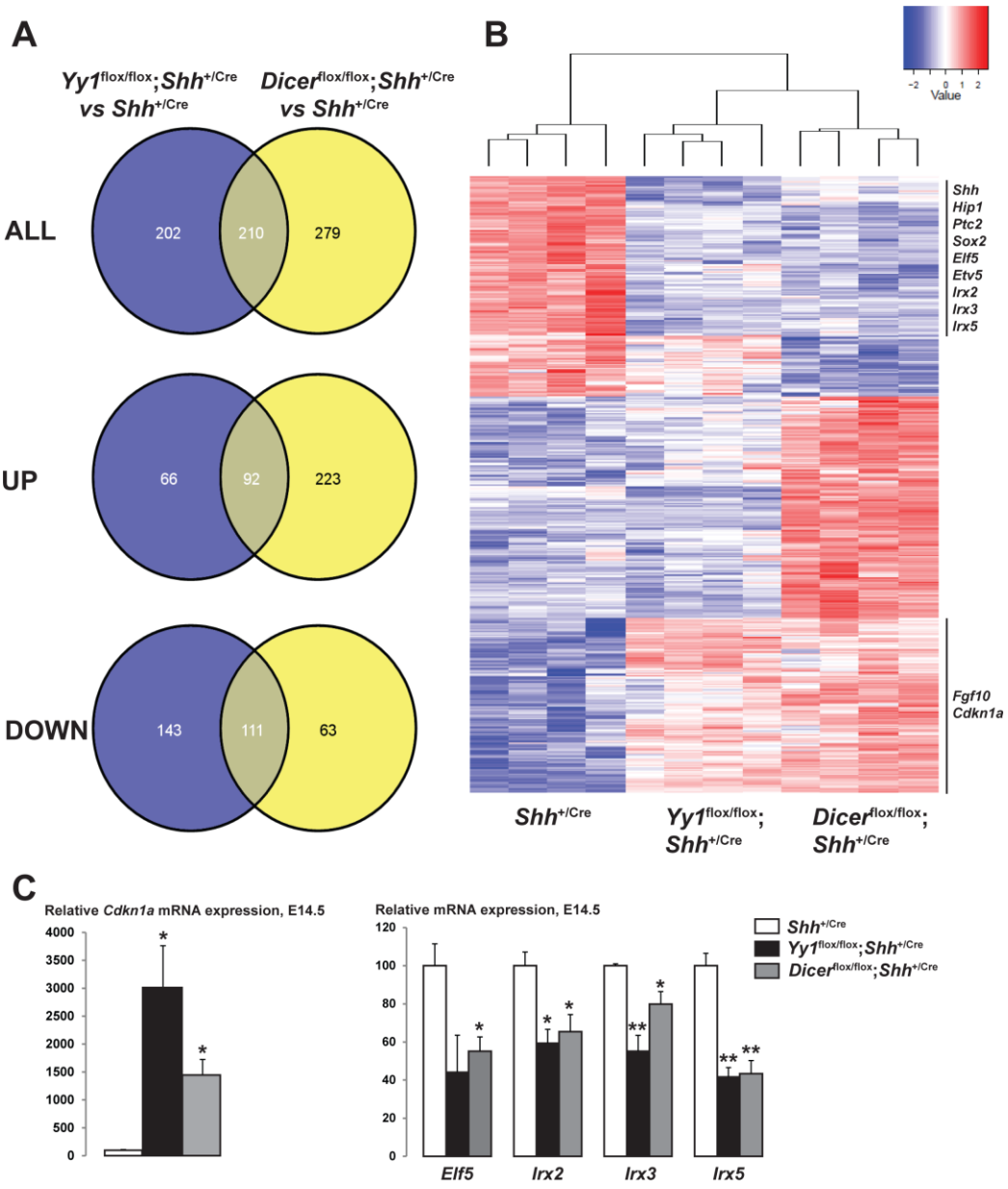

Figure S5. Differential gene expression in lungs from E14.5 *Yy1*$^{flox/flox}$;*Shh*$^{+/Cre}$ and *Dicer*$^{flox/flox}$;*Shh*$^{+/Cre}$ embryos. (A) Venn diagrams representing the overlap of genes differentially expressed (≥1.5-fold change; Benjamini-Hochberg-adjusted $P<0.05$) between genotypes. (B) Heat map analysis displaying deregulated genes (≥1.5-fold; $P<0.05$). The length of the arms of the dendogram reflects the degree of correlation

between the samples. Genes mentioned in the text are indicated on the right. (C) qRT-PCR analyses for *Cdkn1a*, *Elf5*, *Irx2*, *Irx3*, and *Irx5* were performed on biological replicates and confirmed the microarray data. Values are expressed as mean±s.e.m. *P<0.05, **P<0.01.

Table S1. General characteristics of cases

Nº Patient	Final Diagnosis	Age at tissue collection (months)	Localization
1	sudden infant death	4	n.a.
2	sudden infant death	7	n.a.
3	sudden infant death	12	n.a.
4	sudden infant death	10	n.a.
5	sudden infant death	7	n.a.
6	CCAM type I	18	Left lower lobe
7	CCAM type I	1.5	Left superior lobe
8	CCAM type I	11.5	Right lower lobe
9	CCAM type II	16	Left lower lobe
10	CCAM type I	18	Right basal pyramid
11	CCAM type I	22	Left lower lobe
12	CCAM type I	18	Right lower lobe
13	CCAM type I	21	Left lower lobe
14	CCAM type I	20	Left lower lobe
15	PPB type I DICER1 status: unknown	36	Left lower lobe
16	PPB type I DICER1 status: unknown	3	Left lung
17	PPB type I DICER1: c.3293G>A	1.5	Left lingula
18	PPB type II DICER1: c.2379T>G	24	Right lung
19	PPB type II DICER1: c.5392delA	36	Left lower lobe
20	PPB type III DICER1: c.2040+1G>T	36	Right lower lobe
21	PPB type III DICER1: c.4407_4410delTTCT	48	Right lower lobe

Table S2. List of primary and secondary antibodies used for IHC, IF and ChIP

Antigen	Antibody/clone	Reference	Source	Dilution
IHC and IF analyses				
ABCA3	rabbit polyclonal	WRAB-ABCA3	Seven Hills Bioreagents, Cincinnati, OH, USA	1:500
Acetylated tubulin	mouse monoclonal/ clone 6-11B-1	T6793	Sigma Aldrich, Oakville, ON, Canada	1:2000
Active-caspase3	rabbit polyclonal	9661	Cell Signaling, Danvers, MA, USA	1:200
Aquaporin5	rabbit polyclonal	AB78486	Abcam, Toronto, ON, Canada	1:500
αSMA	rabbit polyclonal	AB5694	Abcam, Toronto, ON, Canada	1:300
BrdU	mouse monoclonal/ clone 131-14871	MAB4072	Millipore, Billerica, MA, USA	1:1000
CC10	goat polyclonal		Dr. G. Singh, Georgia Regents University Medical Center, GA, USA	1:500
Cyclin D1	rabbit monoclonal/ clone SP4	RM-9104-S1	Thermo Fisher Scientific, Waltham, MA, USA	1:200
E-cadherin	mouse monoclonal	36/E-Cadherin	BD Biosciences Pharmingen, Franklin Lakes, NJ, USA	1:200
FOXA2	rabbit polyclonal	WRAB-FOXA2	Seven Hills Bioreagents, Cincinnati, OH, USA	1:2000
Ki67	mouse monoclonal/ clone MM1	NCL-L-Ki67-MM1	Leica Biosystems, Concord, ON, Canada	1:200
NKX2-1	rabbit polyclonal	WRAB-TTF1	Seven Hills Bioreagents, Cincinnati, OH, USA	1:3000
p63	mouse monoclonal clone 4A4	sc-8431	Santa Cruz, Santa Cruz, CA, USA	1:100
PECAM-1	rat monoclonal/ clone 13.3	557355	BD Biosciences Pharmingen, Franklin Lakes, NJ, USA	1:75
pERK	rabbit monoclonal	4370	Cell Signaling, Danvers, MA, USA	1:200
pHH3	rabbit monoclonal	9701	Cell Signaling, Danvers, MA, USA	1:200
proSP-C	rabbit polyclonal	AB3786	Millipore, Billerica, MA, USA	1:1500
SOX2	rabbit monoclonal	3728	Cell Signaling, Danvers, MA, USA	1:150
SOX9	rabbit polyclonal	sc-20095	Santa Cruz, Santa Cruz, CA, USA	1:100
T1α	syrian-hamster/ clone 8.1.1.		Hybridoma Bank, IO, USA	1:1000
Vimentin	rabbit monoclonal/ clone D21H3	5741	Cell Signaling, Danvers, MA, USA	1:200
YY1	rabbit polyclonal	sc-1703	Santa Cruz, Santa Cruz, CA, USA	1:300
Biotinylated goat anti-rabbit		BA-1000	Vector Laboratories, Burlington, ON, Canada	1:300
Biotinylated swine anti-goat		CLCC50015	Cedarlane, Burlington, ON, Canada	1:300
Biotinylated goat anti-syrian hamster		107-065-142	Cedarlane, Burlington, ON, Canada	1:300
Biotinylated goat anti-rat		112-065-062	Cedarlane, Burlington, ON, Canada	1:500
Biotinylated goat anti-mouse		115-065-003	Cedarlane, Burlington, ON, Canada	1:500
Donkey anti-rabbit, Alexa Fluor 594 conjugate			Molecular Probes, Eugene, OR, USA	1:250
ChIP assay				
YY1	rabbit polyclonal	sc-1703	Santa Cruz, Santa Cruz, CA, USA	
Histone H3	rabbit polyclonal	ab1791	Abcam, Toronto, ON, Canada	
IgG	-	sc-2027	Santa Cruz, Santa Cruz, CA, USA	

Table S3. List of primer sequences

(A) qRT-PCR		
Gene	**Sequence (5'-3')**	**Fragment size (bp)**
Bmp4	F- AGCGTCCCGCCAGCCGA R- CGGAGCTCTGCCGAGGAG	148
Cdkn1a	F- TCTCAGGGCCGAAAACGG R- ACTTCAGGGTTTTCTCTTGCAG	90
Dicer	F- CGCCTCCTACCACTACAACA R- AGAGCGCAAGTCAGTCAAGA	145
Elf5	F- ACATTCGCTCGCAAGGTTAC R- GTTCGGCTGTGACAGTCTTG	127
Etv4	F- GTCACTTCCAAGAGACGTGG R- GGGGCTATGGAAAGAGTTTTCTG	98
Etv5	F- TGAGAGGCGGGTATTTCTCC R- CCCTCTCGATACATGGTGGG	139
Fgf9	F- TATCCAGGGAACCAGGAAAGAC R- CAGGCCCACTGCTATACTGATAAA	70
Fgf10	F- TCAAAGCCATCAACAGCAACTATT R- CTCTTTCAGCTTACAGTCGTTGTTAAA	95
Foxf1	F- AGCAGCCATACCTTCACCAA R- CTGGGCGACTGTGAGTGATA	82
Foxp1	F- AAAAGACAAAGAGCGCCTGC R- CAGACTTGGAGAGGGTGACA	116
Foxp2	F- ATGCATTGGATGACCGAAGC R- AGTGGGTCATCATCGCTTGA	114
Foxp4	F- GCAGCTGACGCTAAATGAGA R- TCCACACGGACGAAACACTT	129
Hdac1	F- CGAATCCGCATGACTCACAA R- GTCATCTCCTCAGCATTGGC	95
Hdac2	F- ATGGCGTACAGTCAAGGAGG R- GGGATGACCCTGGCCATAAT	90
Hip1	F- CACTTCAACAGCACCAACCA R- AGTAGGATGTCGATCCACGG	87
Hoxa5	F- CCCAGATCTACCCCTGGATG R- GGCATGAGCTATTTCGATCCT	173
Hoxb5	F- TATTCCCCTGGATGAGGAAG R- GGGTCAGGTAGCGATTGAAG	135
Irx2	F- CCGTCCTACGTGGGCTC R- GGTCGTTGAGCTGGTATGGA	106
Irx3	F- GGTTACGGCGCCTTCCT R- AGGGCTGTCCTTCAGCTC	84
Irx5	F- AACTCGCACCTCCAGTACG R- TATCCCAAGGAACCTGCCAT	110
Ptc1	F- GCCTCATTGGGATCAAGCTG R- GCATAGCCCTGTGGTTCTTG	135
Rpl19	F- GATCATCCGCAAGCCTGTGA R- GCATCCGAGCATTGGCAGTA	122
Shh	F- TGACTCAGAGGTGCAAAGACA R- ACTCCTCTGAATGATGGCCG	120

Spry2	F- AAGCCGCGATCACGGAGTTCA R- CTGCAGCAAAGGCTGCGACC	113
Yy1	F- CATGTGGTCCTCGGATGAAA R- GGGAGTTTCTTGCCTGTCATA	117

(B) ChIP		
Gene	**Sequence (5'-3')**	**Fragment size (bp)**
Sfrs10	F-TTTCTCCGCTTCACCCTTGGA R-AACGGTATCTTCTTTCGCCGTTGGA	175
Rcor3	F-GTCTCAGCTGAAGGAATTTGGCCT R-GCCATCCTCATAGCTCCTGTCAAA	157
Shh #1	F-CTGGAGAGCTTGTGAGACAG R-AGTCTTTCTCAGGGTTAACATCA	113
Shh #2	F-CGAAGACCAAATAAGAGCCAGA R-CTGGATCAAGAACAGTGGGT	104
Shh #3	F-CCTAAGCTGCCAGTGTTCTATG R-GAACCAAGTCACCTCCTTCTTC	97
Shh #4	F-CCCTGGAGGCATAGTCCTG R-CCGAAGGCAGAGTGAGGA	79
Shh #5	F-CTGTCCAGAGTGAGCACAAG R-CTCCATTTCCCAGTGTGAGG	103
ctl locus	F-AGACCTGGATATAGTTAAGATGCG R-ACCCTGTGTTCCATCCAATAG	83